JAERI-M
83-147

INVESTIGATION OF REFLOOD MODELS BY COUPLING REFLA-1D AND MULTI-LOOP SYSTEM MODEL

September 1983

Jun SUGIMOTO and Yoshio MURAO

日本原子力研究所
Japan Atomic Energy Research Institute

JAERI-Mレポートは，日本原子力研究所が不定期に公刊している研究報告書です。
入手の問合わせは，日本原子力研究所技術情報部情報資料課（〒319-11茨城県那珂郡東海村）あて，お申しこしください。なお，このほかに財団法人原子力弘済会資料センター（〒319-11茨城県那珂郡東海村日本原子力研究所内）で複写による実費頒布をおこなっております。

JAERI-M reports are issued irregularly.
Inquiries about availability of the reports should be addressed to Information Section, Division of Technical Information, Japan Atomic Energy Research Institute, Tokai-mura, Naka-gun, Ibaraki-ken 319-11, Japan.

編集兼発行　日本原子力研究所
印　　刷　㈱高野高速印刷

JAERI-M 83-147

Investigation of Reflood Models by Coupling REFLA-1D and Multi-loop System Model

Jun SUGIMOTO and Yoshio MURAO

Department of Nuclear Safety Research,
Tokai Research Establishment, JAERI

(Received August 12, 1983)

A system analysis code REFLA-1DS was developed by coupling reflood analysis code REFLA-1D and a multi-loop primary system model. The reflood models in the code were investigated for the development of the integral system analysis code.

The REFLA-1D, which was developed with the small scale reflood experiment at JAERI, consists of one-dimensional core model and a primary system model with a constant loop resistance. The multi-loop primary system model was developed with the Cylindrical Core Test Facility of JAERI's large scale reflood tests. The components modeled in the code are the upper plenum, the steam generator, the coolant pump, the ECC injection port, the downcomer and the broken cold leg nozzle.

The coupling between the two models in REFLA-1DS is accomplished by applying the equivalent flow resistance calculated with the multi-loop model to the REFLA-1D. The characteristics of the code is its simplicity of the system model and the solution method which enables the fast running and the easy reflood analysis for the further model development.

A fairly good agreement was obtained with the results of the Cylindrical Core Test Facility for the calculated water levels in the downcomer, the core and the upper plenum. A qualitatively good agreement was obtained concerning the parametric effects of the system pressure, the ECC flow rate and the initial clad temperature. Needs for further code improvements of the models, however, were pointed out. These include the problem concerning the generation rate of the steam and water droplets in the core in an early period, the effect of the flow oscillation on

---

The work was performed under contract with the Atomic Energy Bureau of Science and Technology Agency of Japan

the core cooling, the heat release from the downcomer wall, and the stable system calculation.

Keywords: Reactor Safety, Reflood, PWR,LOCA, System Model, CCTF, Analysis Code

JAERI－M 83－147

REFLA－1Dと多ループシステムモデルの結合による再冠水モデルの検討

日本原子力研究所東海研究所安全工学部
杉本　純・村尾　良夫

（1983年8月12日受理）

再冠水解析コードREFLA－1Dと多ループシステムモデルを結合して，システム解析コードREFLA－1DSを開発した。本コードにより，総合システム解析コードのための再冠水モデルの検討を行った。

REFLA－1Dは，原研小型再冠水実験に基づいて開発された，一次元炉心熱水力モデルと一次系一定流動抵抗モデルとを組合せたコードである。多ループシステムモデルは，原研円筒炉心試験に基づいて開発され，上部プレナム，蒸気発生器，冷却材ポンプ，ECC注入口，ダウンカマおよび破断コールドレッグノズルがモデル化されている。

REFLA－1DSにおいては，多ループシステムモデルで計算された等価流動抵抗を，REFLA－1Dに適用することにより両者を結合している。本コードの特徴は，単純なシステムモデルと解法により，高速かつ簡便な再冠水モデルの検証が可能なことである。

本コードによる円筒炉心試験解析の結果，ダウンカマ，炉心および上部プレナム内水位の計算値は実測値とほぼ良い一致を示した。また系圧力，ECC流量および被覆管初期温度のパラメータ効果に関しても，定性的に良い一致が得られた。ただし，初期における炉心からの蒸気・水滴の発生量，炉心冷却に及ぼす流体振動の影響，ダウンカマ壁からの放熱およびシステム計算の安定性等について，改善すべき点のあることが指適された。

本報告書は，電源開発促進対策特別会計法に基づき，科学技術庁からの受託によって行った研究の成果である。

Contents

目　　次

List of tables

List of figures

1. Introduction

The present report describes a system analysis code namded REFLA-1DS for the reflood phase of a loss-of-coolant accident (LOCA) in a PWR. The code consists of the one-dimensional reflood analysis code REFLA-1D[1] and the multi-loop system models.[2] The coupling method of the core and system models, an application example and the calculated results are described.

In the safety analysis of a LOCA, it is important to evaluate the temperature history of the fuel cladding during the reflood phase. In order to investigate the thermo-hydraulic behavior during the reflood phase, many experimental works have been performed. For example, FLECHT experiments[3] have generated the heat transfer correlations and fluid flow data used for the licensing of PWRs. The large scale reflood test facilitties[4][5] at Japan Atomic Energy Research Institute (JAERI) have revealed the two and three dimensional thermo-hydraulic characteristics in the core. It is shown that the core cooling is significantly enhanced with the higher flooding rate due to the increased vapor generation rate and liquid entrainment.

The flooding rate, on the other hand, is controlled by the balance between the driving head of the downcomer which forces the water into the core, and the back pressure in the upper plenum created by the steam-water mixture flowing from the core exit to the break. This back-pressure or "steam binding" tends to retard the core flooding rate during reflood phase. Thus the core thermo-hydraulics is strongly linked with the system thermo-hydraulics.

In the safety evaluation of the reflood phase of PWRs, the empirical correlations were used for the heat transfer and the carryover rate fraction. The carryover rate is used for the calculation of the core inlet flow conditions. This method is valid for the quasi-steady-state analysis within the experimental range of the correlations. For a flexible application to the safety analysis, a best-estimate computer code for the reflood phase was intended to be developed based on the physical understanding of the phenomena.

As a first stage, a one-dimensional core thermo-hydraulic code[1] was developed for a single coolant channel in a reactor core with bottom coolant injection at a constant flow rate. A one-dimensional system analysis code REFLA-1D[6] was then developed by coupling the one-dimensional

core model and a primary system model. The code was evaluated using the one-dimensional reflood system experiments conducted at JAERI.[7] The core thermo-hydraulic models have since been inproved based on the small scale reflood experiment at JAERI and other existing reflood experiments. The version REFLA-1D/mode 3[8][9] is utilized as a base for the present core model.

In order to investigate the core and system behaviors during reflood phase, the integral tests with the Cylindrical Core Test Facility (CCTF)[4] have been conducted at JAERI. The facility is designed to model a full-height core and four primary loops with simulated full components of PWRs. The CCTF tests showed that the main loop pressure drop is realized at the pump section where the almost single phase vapor is flowing and that the system responses can be regarded as nearly quasi-steady state in the reflood phase.

The multi-loop system component model in the present code has been developed based on the CCTF test results. The coupling of the core model with the multi-loop system model is based on the equivalent loop flow resistance in the single loop system, which is used in the scheme of the REFLA-1D. The characteristics of the code is its simplicity of the system model and the solution method that enables the fast running of the code and the easy reflood analysis. The code can be utilized to improve and to testify the models as a pilot code for the further integral system analysis code.

2. Coupling of core and system component models

In the present code, the coupling of the core and the multi-loop system component models is simply accomplished by the use of the equivalent K-factor in the single loop. This is based on the CCTF test results,[4] i.e., the main loop pressure drop is realized at the pump section where the almost single phase vapor is flowing and the system responses can be regarded as nearly the quasi-steady state. This means that the loop flow resistance can be approximately expressed by an equivalent K-factor in the simplified single loop with the single phase vapor due to the slow transient in the reflood phase.

2.1 Basic assumption

The present code utilizes the same scheme shown in Fig. 2.1 as in the REFLA-1D system code[6], in which the followings are assumed:

(1) Single phase liquid forms a U-tube column between the lower part of the core and the downcomer through the lower plenum.

(2) The motion of the water column in a reactor vessel is one-dimensional.

(3) Both ends of the water column are connected with a primary loop where the single phase vapor is flowing.

In the present code, the energy equation is considered for the multi-loop system in order to calculate the temperature of the two-phase flow. The mass and momentum equations are based on the single loop system shown in Fig. 2.1. The multi-loop system is related to the single loop system through the equivalent K-factor of the primary loop. This scheme allows a simple treatment of the solution of the momentum equation. The direct leak path or the vent valve path from the upper plenum to the downcomer can easily be modeled in this scheme. The core or system thermo-hydraulic model can easily be verified due to the simplicity and the fast running of the code.

2.2 Basic equations

The basic equations for the single loop system shown in Fig. 2.1 are given in the following.

Conservation equations of the mass in the downcomer and the core are

$$W_D^I = A_D \rho_\ell \dot{x} + A_I \rho_\ell U_I + W_{\ell D} \tag{1}$$

$$A_I \rho_\ell U_I = A_c \rho_\ell \dot{y} + W_{gc}^o + W_{\ell c}^o \tag{2}$$

where W_D^I is the sum of the injected mass flow rate into the lower part of the downcomer; W_{gc}^o and $W_{\ell c}^o$ are the steam and liquid mass flow rates at the core outlet, respectively; The downcomer over flow rate $W_{\ell D}$ is expressed using the maximum downcomer length x_{max}.

Conservation equations of the momentum in the primary loop, the downcomer, the lower plenum (downcomer-core connecting port) and the core are as follows;

$$P_U - P_s = (K_L/2\ \rho_{g\ sat})(W_L/A_L)^2 \tag{3}$$

$$\rho_\ell \frac{d}{dt}(x \dot{x}) = P_D - P_s - \rho_\ell g x - K_D(\rho_\ell/2)|\dot{x}|\dot{x} \tag{4}$$

$$\rho_\ell \frac{d}{dt}(L_I U_I) = P_D - P_I - K_I(\rho_\ell/2)|U_I|U_I \tag{5}$$

$$\rho_\ell \frac{d}{dt}(y \dot{y}) = P_I - P_U - \Delta P_U - \rho_\ell g y - K_c(\rho_\ell/2)\left|\frac{A_I}{A_C}U_I\right|\frac{A_I}{A_C}U_I \tag{6}$$

In the above formulation, the acceleration loss is neglected in the primary loop pressure drop, since the vapor density is much smaller than the liquid density in the reflood phase. The total frictional pressure loss is assumed to be represented by a K-factor loss coefficient.

In the upper plenum, the simple ideal gas equation is assumed to hold for the saturated steam, i.e.,

$$V_U \frac{dP_U}{dt} = R\ T_U\ (W_{gc}^o - W_L) \tag{7}$$

where V_U and T_U are the volume and the temperature of the upper plenum, respectively, R the gas constant of the steam.

The unkown five variables in Eqs. (3) through (7) are combined into a vector X defined as

$$X = X(x, y, U_I, P_D, P_I) \tag{8}$$

The core outlet variables W^o_{gc} and $W^o_{\ell c}$ are calculated by the core component model, and the differential pressure ΔP_U in the upper plenum is calculated by the upper plnum component model. Also the injected mass flow rate W^I_D and the system pressure P_S are given as a boundary condition. Thus the simultaneous differential equations described above are solvable.

2.3 Solution method

The basic equations given in Eqs. (1) through (7) can be converted into a simple form:

$$\ddot{x} = \{P_U + \Delta P_U - P_S)/\rho_\ell + (y - x)g + \dot{y}^2 - \dot{x}^2$$
$$+ \frac{1}{2}\left(K_I|U_I|U_I + K_C\left|\frac{A_I}{A_C}U_I\right|\frac{A_I}{A_C}U_I - K_D|\dot{x}|\dot{x}\right)$$
$$+ \frac{1}{g\,\rho_\ell}\left\{\left(\frac{L}{A_I} + \frac{y}{A_C}\right)\frac{d}{dt}W^I_D - \frac{y}{A_C}\frac{d}{dt}(W^o_{gc} + W^o_{\ell c})\right\}$$
$$/\left(x + y\frac{A_D}{A_C} + L\frac{A_D}{A_I}\right) \quad , \tag{9}$$

Here U_I can be expressed as a function of x using Eq. (1). Therefore, if we define the variable $y_i (i = 1 \sim 4)$ such that,

$$y_1 = x,\ y_2 = \dot{x},\ y_3 = y,\ y_4 = P_u$$

Eqs. (1)(2)(7) and (9) can be written in the following form:

$$\frac{d}{dt}y_i = F_i(y_1, y_2, y_3, y_4) \tag{10}$$

This is a simultaneous differential equation concerning $y_i (i = 1 \sim 4)$. The Runge-Kutta-Gill method is used in the code to numerically solve the differential equation (10).

2.4 Coupling of single and multi-loop systems

The method of coupling of single and multi-loop systems is described in the following. The schematic diagram is shown in Fig. 2.2. The single phase vapor is assumed to flow in the primary loop except for the broken cold leg nozzle. The pressure drop across the broken cold

leg nozzle ΔP_{BCN} ($= P_S - P_0$) is calculated with the component model described in 3.2.7.

The differential pressure between the upper plenum and the upper part of the downcomer strongly affects the core flooding rate, and hence it must be conserved between the two schemes:

$$P_u - P_s = \frac{1}{2\rho_g} \cdot K_L \cdot \left(\frac{W_L}{A_L}\right)^2 = \frac{1}{2\rho_g} \cdot K_{Ii} \cdot \left(\frac{W_{Ii}}{A_{Ii}}\right)^2 \quad (i = 1 \sim N) \tag{11}$$

where K_L is the equivalent K-factor in the single loop system, K_{Ii} the K-factor of i-th intact loop and N the total number of the intact loops in the multi-loop system.

The total mass effluent rate from the upper plenum should also be conserved between the two scheme i.e.,

$$W_L = W_B + \sum_{i=1}^{N} W_{Ii} \equiv W_B + W_I \quad . \tag{12}$$

The differential pressure between the upper plenum and the break point in the multi-loop system is expressed as,

$$\frac{1}{2\rho_g} K_B \left(\frac{W_B}{A_B}\right)^2 = \frac{1}{2\rho_g} K_{Ii} \left(\frac{W_{Ii}}{A_i}\right)^2 + \Delta P_{BCN} \quad . \tag{13}$$

The equivalent K-factor K_L of the single loop is easily derived from Eqs. (11) through (13) as,

$$K_L = K_I \frac{1}{\left[1 + \sqrt{\frac{K_I}{K_B}} \left(\frac{A_B}{A_L}\right) \sqrt{1 + \Delta P_{BCN} / \left\{\frac{1}{2\rho_g} K_I \left(\frac{W_I}{A_L}\right)^2\right\}}\right]^2} \quad , \tag{14}$$

where K_I is the K-factor of a combined intact loop defined by

$$\frac{1}{\sqrt{K_I}} = \frac{1}{A_L} \sum_{i=1}^{N} \frac{A_{Ii}}{\sqrt{K_{Ii}}} \tag{15}$$

The injected mass flow rate W_D^I in Eq. (1) is related to the mass flow rates of the multi-loop system as,

$$W_D^I = W_{ECCLP} + W_o + W_{FB} \tag{16}$$

The calculation procedure used in the code is shown in Fig. 2.3. The system variable X in the single loop at time t + Δt is calculated by explicity solving Eq. (10). The core outlet variables W_{gc}^o and $W_{\ell c}^o$ at the previous time t and the equivalent K-factor determined by Eq. (14) are used in this step. The multi-loop system variables at time t + Δt are then calculated by solving the mass and energy equations with the multi-loop system component model. Finally, the core thermo-hydraulic variables at time t + Δt are updated with the core model. In this step, the flooding rate W_c^I, the inlet water temperaure $T_{\ell c}^I$ and the pressure at the core inlet P_I are used as a core inlet boundary condition.

2.5 Smoothing procedure

The solution method used in the code is so-called a forward differential scheme with no iteration. This is used in the core and multi-loop system models in order to reduce the running time. This method, as well known, sometimes causes the numerical instability. In the present coupling scheme of the core and the system component models, the fluctuation of the liquid and steam mass flow rates at the core boundary can result in the growth of the oscillation of the system variables.

The source of this numerical disturbance is in the core model, in which the core outlet variables are sensitively affected by the change of the flow pattern, the advance of the quench front across the node interface and the change of the inlet flooding rate. Figure 2.4 (a) shows an example of the core outlet varibales (W_{gc}^o and $W_{\ell c}^o$) calculated with a constant feed condition by REFLA-1D core model. The spiky behavior or the numerical disturbance at the core outlet is observed even in the completely steady state inlet condition. This disturbance is found to be remarkably enhanced when the core inlet flow contains fluctuations as shown in Fig. 2.4(b).

This disturbance needs to be effectively damped for the stable calculation of the system variables such as the mass flow rates. In

the present code, the numerical low-pass filter, which is analogous to the R-C filter in electronics shown in Fig. 2.5, is utilized for that purpose:

$$V_1 = \frac{1}{2\pi f_o} \frac{d V_2}{dt} + V_2 \quad , \tag{17}$$

where V_1 is the input voltage to the filter and V_2 the output voltage. The cut off frequency f_o (= $1/2\pi$ RC) is determined in consideration of the typical oscillation frequency expected in the reflood phase ($0.2 \sim 0.4$ H_z). The numerical low-pass filters are utilized for the core outlet mass flow rates (W^o_{gc} and $W^o_{\ell c}$) and the broken cold leg pressure drop (ΔP_{BCN}). An example of the smoothed core outlet mass flow rates by the filter are also shown in Figs. 2.4(a) and (b).

The use of the low-pass filter physically means that the reflood phenomena is treated under the quasi-steady state condition neglecting the rapid change of the system variables. This corresponds to the present core and system component models which are developed with the steady state condition. The calculated average values are thus to be analysed, but the calculated dynamical behavior with large frequency is not necessarily correct. Since the detailed mass balance between each time step is not always conserved due to the phase change of the filter output, the improvements of the core model and the coupling method are required for the more stable and reasonable calculation.

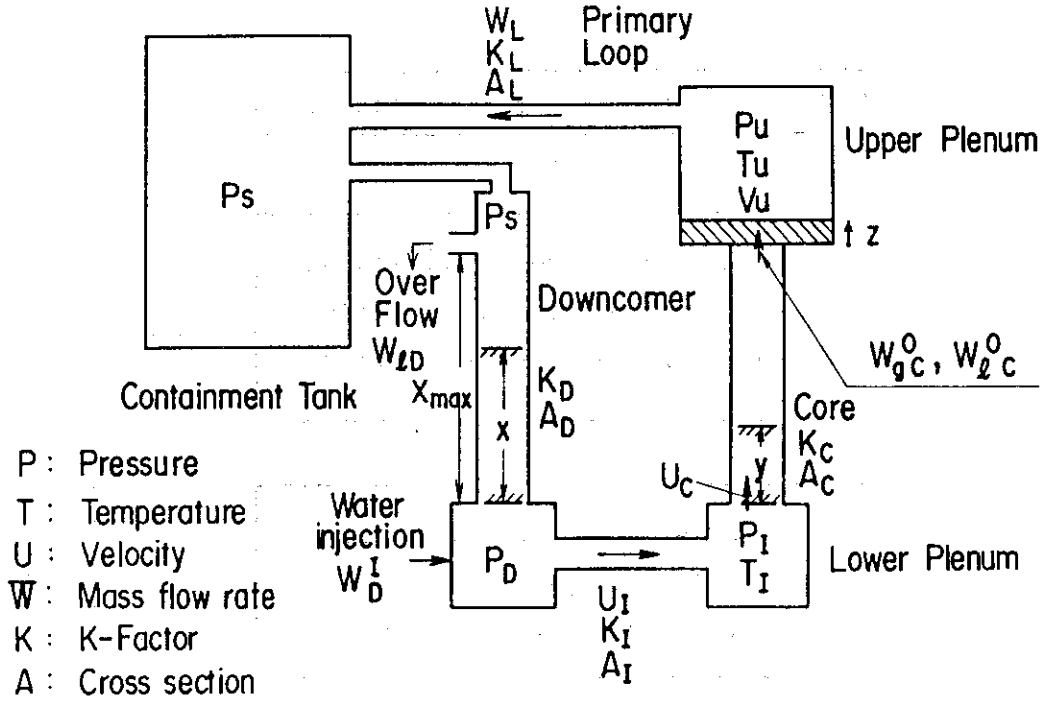

Fig. 2.1 Schematic of one-dimensional system

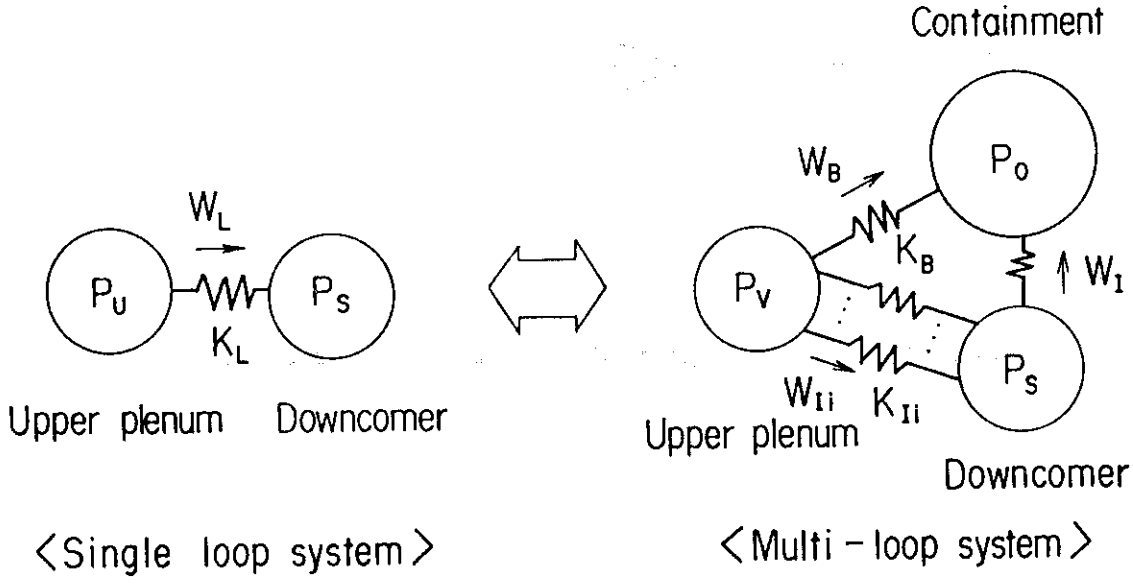

Fig. 2.2 Coupling of single and multi-loop systems

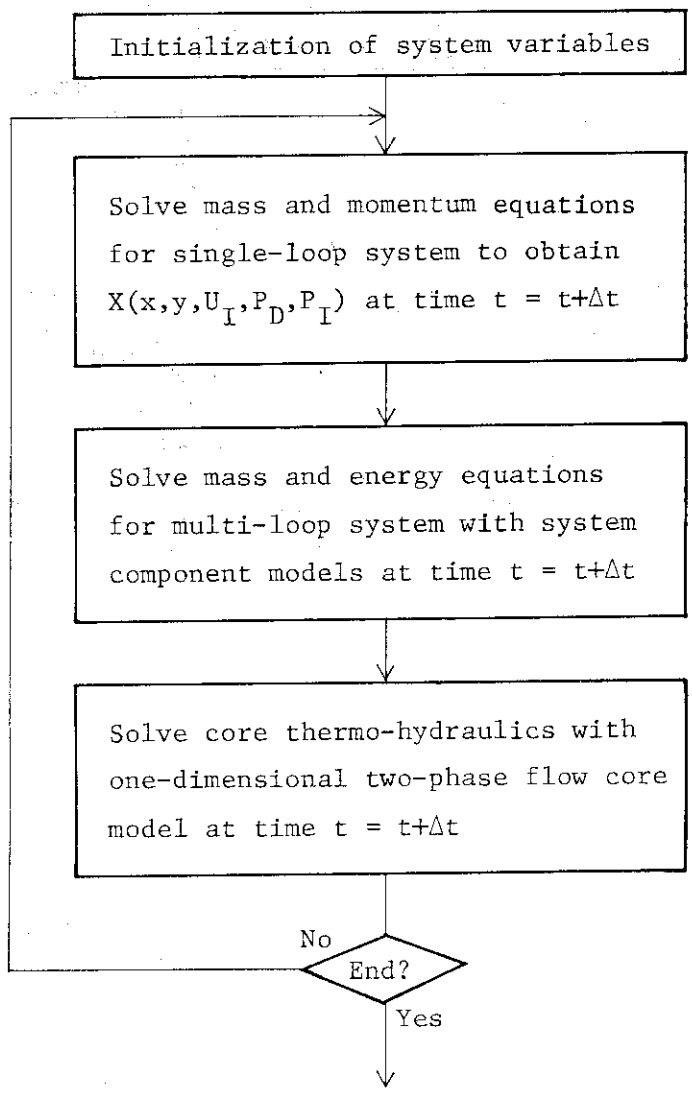

Fig. 2.3 Flow diagram of calculational procedure

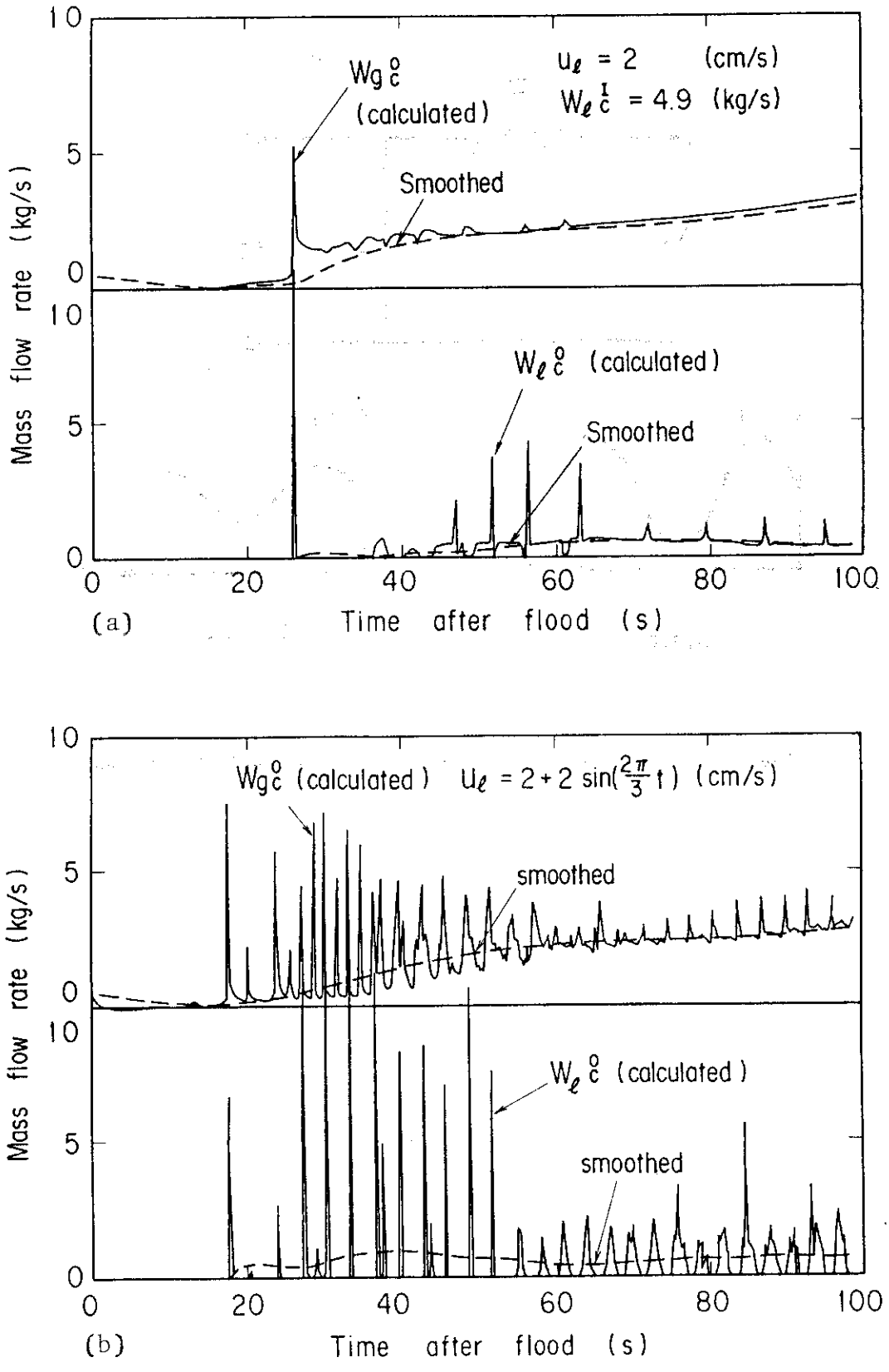

Fig. 2.4 Example of calculated core outlet variables and smoothed data

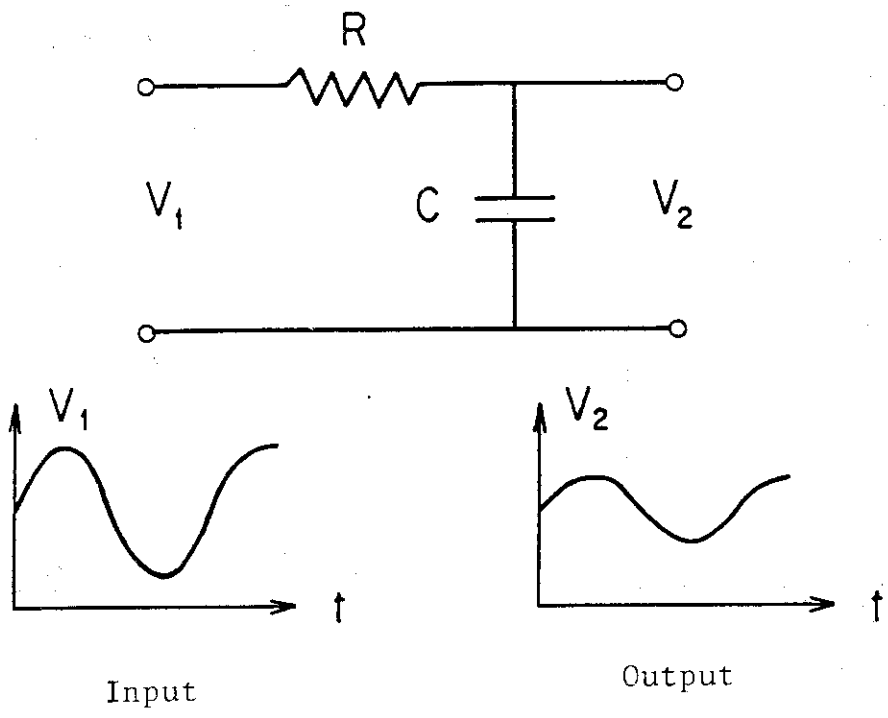

Fig. 2.5 Schematic of low-pass filter for smoothing

3. Model description

The component models used in REFLA-1DS are briefly described in this chapter. The code consists of the core model and the multi-loop primary system component model. The core model was developed with the existing small scale reflood experiments, whereas the multi-loop primary system component model was developed with the CCTF test results.

3.1 Core model

The core model is based on the one-dimensional non-equilibrium two-phase flow. The flow patterns assumed in the core are a single phase liquid and vapor flows, a saturated two-phase flow, a transition flow, a subcooled film boiling and a dispersed flow regions. The details of the core model is reported in references (1) and (4). The present version of the core model REFLA-1D/mode 3[8] includes the following two major modifications:

(1) Correlation of the quench front velocity

The correlation of the quench front velocity U_Q is modified considering the case of the low clad temperature and the pressure dependence[10]:

$$U_Q^{-1} = f(x)g(T_1) + \{1 - f(x)\}g(T_2) \tag{18}$$

where

$$f(x) = \begin{cases} 1 & (T_Q \geqslant T_C) \\ (T_Q - T_2)/T_C - T_2) & (T_Q < T_C) \end{cases} \tag{19}$$

$$g(T) = \begin{cases} \dfrac{C_p \rho (T_Q - T)}{\phi(1 + 2.778 \times 10^{-5} \Delta T_{sub})} & (T_Q > T_2) \\ 0 & (T_Q \leq T_2) \end{cases} \tag{20}$$

$$T_1 = 594.05 + 2.417 \times 10^{-6} P \tag{21}$$

$$T_2 = 480.0 + 8 \times 10^{-5} P$$

$$\phi = 2.97 \times 10^5 + 5.74 P \tag{22}$$

The temperature T_Q is the quench temperature and T_C the contact temperature between the clad and the liquid. Equation (20) is the original form of the correlation of the quench front velocity[11]. Equation (18) means that the quench in the low clad temperature occurs in a statistical way for the contact of the water film to the clad surface.

(2) Modeling of the development of water droplets

It is assumed that the fine water droplets are generated at the quench front. Two cases are supposed to be possible concerning the development of the droplets above the quench front.

1) Case 1: The water droplet dispersed flow is maintained above the quench front. The diameter of the droplet D_d is determined by the critical Weber number W_{ec} in the dispersed flow:

$$D_d = \frac{W_{ec} \cdot \sigma}{\rho_g \cdot \Delta U^2} \tag{23}$$

2) Case 2: The water droplets begin to unite each other to form a larger size of droplets. The flow above the quench front thus becomes the transition flow from the dispersed flow in a short distance above the quench front.

It was found that Case 1 well describes the reflood situation when the flooding rate is very low (less than ∿2 cm/s), the temperature of the flow housing is high (greater than ∿500°C) and the upper tie plate is absent. Whereas Case 2 describes the opposite situation fairly well. Although the detailed mechanism of this switching between the two cases is not well understood, Case 2 was found to be widely applicable for the system reflood experiments such as FLECHT-SET[12] or CCTF[13] test.

3.2 System componenet model

The primary loop system components modeled in REFLA-1DS are the upper plenum, the coolant pump, the ECC injection port, the broken cold leg nozzle, the downcomer annulus and the downcomer. The present version selects the simplest model for the system component based on the reflood system experiments[12][13].

3.2.1 Upper plenum

The schematic of the upper plenum is shown in Fig. 3.1. The mass balance relation is written as,

$$W^{o}_{gc} + W^{o}_{\ell c} = \dot{M}_{U} + W^{I}_{gL} + W^{I}_{\ell L} + W_{FB} \quad , \tag{24}$$

where the core outlet vapor and liquid mass flow rates W^{o}_{gc} and $W^{o}_{\ell c}$, respectively are calculated with the core model described in 2.1. It is assumed that the two-phase mixture in the upper plenum is thermally equilibrium. The loop mass flow rates W^{I}_{gL} and $W^{I}_{\ell L}$ are expressed with the total loop mass flow rate W_{L} in Eq.(3):

$$W^{I}_{gL} + W^{I}_{\ell L} = W_{L} \quad . \tag{25}$$

The water fall back mass flow rate W_{FB} in Eq. (25) is calculated with the correlation developed by Bankoff et al.[14] which is expressed as

$$W_{FB} = (2.0 - H_{g}^{\frac{1}{2}})^{2} \quad , \tag{26}$$

where

$$H_{g} = \frac{W^{o}_{gc}}{(g\ \rho_{g}) \cdot A_{h}} \left[\rho_{g} / \{g\ w(\rho_{\ell} - \rho_{g})\}\right]^{\frac{1}{2}} \quad ,$$

$$w = D_{h}^{1-\beta} \left[\sigma / \{g\ (\rho_{\ell} - \rho_{g})\}\right]^{\frac{\beta}{2}} \quad ,$$

$$\beta = \tanh \left(\frac{2\pi}{d_{h}} \frac{A_{c}}{A_{h}} \right) \quad .$$

Here A_{h} denotes the total flow area of the holes at the upper tie plate, D_{h} the diameter of the hole, d_{h} the thickness of the hole and A_{c} the core flow area. The liquid carry-over $W^{I}_{\ell L}$ from the upper plenum to the hot legs is calculated with the upper plenum model developed by Iguchi et al.[15] The carry-over mass flow rate consists of two terms. One is the contribution of the core outlet liquid, and the other expresses the re-entrainment from the water pool in the upper plenum.

The correlation is written as follows:

$$W^{I}_{\ell L} = W_{1} + W_{2} \quad , \tag{27}$$

where $W_1 = \eta_U \cdot (1 - a_1) \cdot W^o_{\ell C}$,

$$a_1 = \frac{M_U}{h_1' \cdot \rho_\ell \cdot A_U} \quad ,$$

and

$$W_2 = \begin{cases} W^o_{\ell C} - W_{FB} & (\Delta P_U > \Delta P_{max}) \\ \eta_U \cdot \dfrac{\Delta P_U}{\Delta P_{max}} \cdot \dfrac{\rho_\ell \cdot A_U}{300} & (\Delta P_U < 0.9\ \Delta P_{max}) \\ \text{Interpolation} & (0.9\ \Delta P_{max} \leq \Delta P_U \leq \Delta P_{max}) \end{cases}$$

where η_U is the upper plenum de-entrainment coefficient and h_1' the critical water level for which W_1 is effective. The maximum differential pressure in the upper plenum ΔP_{max} is defined as,

$$\Delta P_{max} = h_{max}\, \rho_\ell (1 - \alpha) \quad , \tag{28}$$

where the void fraction α in the upper plenum is expressed by the correlation developed by Wilson et al.[16]:

$$\alpha = \max\ (\alpha_1, \alpha_2) \quad , \tag{29}$$

where

$$\alpha_1 = 0.851\ X^{0.4382} / \left(\frac{\rho_\ell}{\rho_g}\right)^{0.1798} \left(D_U / \sqrt{\sigma / g(\rho_\ell - \rho_g)}\right)^{0.1067} ,$$

$$\alpha_2 = 0.488\ X^{0.6403} / \left(\frac{\rho_\ell}{\rho_g}\right)^{0.1151} \left(D_U / \sqrt{\sigma / g(\rho_\ell - \rho_g)}\right)^{0.0683} ,$$

$$X = V_{go} / \sqrt{g_c \sqrt{\sigma / g(\rho_\ell - \rho_g)}} \quad ,$$

$$V_{go} = W^o_{gc} / (A_U\, \rho_\ell) \quad .$$

Here D_U denotes the hydraulic diameter in the upper plenum.

The water accumulation rate $\dot{M}_U$ in the upper plenum can then be written using Eqs. (24) and (25) as

$$\dot{M}_U = W^o_{gc} + W^o_{\ell C} - W_L - W_{FB} \quad . \tag{30}$$

The accumulated water at the new fime step M_U^{n+1} is calculated using Eq. (30) i.e.,

$$M_U^{n+1} = M_U^{n} + \Delta t \cdot \dot{M}_U \quad . \tag{31}$$

The mixture water level h' and the differential pressure in the upper plenum ΔP_{up} are calcualted using the updated mass M_U^{n+1}:

$$h' = \frac{M_U^{n+1}}{A_U \cdot \rho_\ell \cdot (1 - \alpha)} \quad , \tag{32}$$

$$\Delta P_U = h' \cdot \rho_\ell \cdot (1 - \alpha) \quad . \tag{33}$$

It is noted that the differential pressure ΔP_U used in the calculation of W_2 in Eq. (27) is evaluated at the previous time step n in the code.

3.2.2 Steam generator

The almost complete superheat of the fluid at the outlet of the steam generator has been observed in CCTF test.[13] This is due to the heat transfered from the secondary side to the primary side of the steam generator. In the present code, the fluid in the primary side is assumed to be all evaporated through the steam generator as the zero-order approximation. The steam temperature at the outlet of the steam generator is set equal to the average temperature of the fluid in the secondary side.

This allows an easy treatment of the momentum and energy balance calculation of the primary loop. The fine water droplets, however, may still be present in the superheated steam flow as observed in the FLECHT-SET experiment[12]. This effect on the system responses is to be carefully investigated. However, the water droplet dispersed flow situation downstream the steam generator can also be considered in a similar manner described in the following sections.

3.2.3 Pump

The primary loop coolant pump acts as a main flow resistance during reflood phase. This steam binding effect is enhanced by the complete evaporation of the water droplets through the steam generators. In the present code, the pressure drops across the pump ΔP_{Pi} and the loop

ΔP_{Li} are assumed to be expressed by the K-factors of the pump and the loop, respectively:

$$\Delta P_{Pi} = \frac{K_{pi}}{2\rho_{gi}} \left(\frac{W_{gLi}}{A_{Li}} \right)^2 \tag{34}$$

$$\Delta P_{Li} = \frac{K_{Li}}{2\rho_{gi}} \left(\frac{W_{gLi}}{A_{Li}} \right)^2 \tag{35}$$

where suffix i denotes the i-th loop, K_{pi} and K_{Li} are the K-factor of the i-th pump, and loop, respectively, W_{gLi} the steam mass flow rate through the loop. The main contribution to K_{Li} is due to the pump flow resistance K_{pi}.

3.2.4 ECC injection port

The schematic of the ECC injection port at the cold leg is shown in Fig 3.2. The flow rate and the temperature downstream the ECC injection port are calculated based on the following assumptions:

(1) The superheated steam from the steam generator is completely mixed with the injected ECC water to form a thermally equilibrium condition.

(2) No reverse flow occurs from the ECC injection port to the steam generator.

The mass and energy balances are then written as,

$$W^I_{gLi} + W_{ECCi} = W^o_{gLi} + W^o_{\ell Li} \quad , \tag{36}$$

$$C_{p\ell i}(\bar{T}_i - T_{sat})(W^o_{gLi} + W^o_{\ell Li})$$

$$= W^o_{gLi}\{h_{fg} + C_{pgi}(T^o_{gLi} - T_{sat})\} + W^o_{\ell Li}\, C_{p\ell i}(T^o_{\ell Li} - T_{sat})$$

$$= W^I_{gLi}\{h_{fg} + C_{pgi}(T^I_{gLi} - T_{sat})\} + W_{ECCi}\, C_{p\ell i}(T_{ECCi} - T_{sat}) \tag{37}$$

The mixture temperature $\bar{T}_i$ defined above can easily be derived using Eqs. (36) and (37):

$$\bar{T}_i = \frac{W^I_{gLi}\{h_{fg} + C_{p\ell i}\, T_{sat} + C_{pgi}(T^I_{gLi} - T_{sat})\} + W_{ECCi}\, C_{p\ell i}\, T_{ECCi}}{C_{p\ell i}(W^I_{gLi} + W_{ECCi})} \tag{38}$$

(a) If $\bar{T}_i$ is less than T_{sat} i.e. the mixture is subcooled

$$\begin{aligned} W^{o}_{gLi} &= 0 \\ W^{o}_{\ell Li} &= W^{I}_{gLi} + W_{ECCi} \\ T^{o}_{gLi} &= T_{sat} \\ T^{o}_{\ell Li} &= \bar{T}_i \end{aligned} \tag{39}$$

(b) If $\bar{T}_i$ is greater than T_{sat}, evaporation of the mixture is considered. The energy flux X of the mixture evaluated at the saturation temperaure is expressed as,

$$X = W^{I}_{gLi}\, C_{pgi}(T^{I}_{gLi} - T_{sat}) - W_{ECCi}\, \{h_{fg} + C_{p\ell}(T_{sat} - T_{ECCi})\}. \tag{40}$$

(i) If X is greater than zero, the liquid is all evaporated to generate superheated steam flow:

$$\begin{aligned} W^{o}_{gLi} &= W^{I}_{gLi} + W_{ECCi} \\ W^{o}_{\ell Li} &= 0 \\ T^{o}_{gLi} &= T_{sat} + \frac{X}{C_{pg}(W^{I}_{gLi} + W_{ECCi})} \\ T^{o}_{\ell Li} &= T_{sat} \end{aligned} \tag{41}$$

(ii) If X is less than zero, the mixture is a saturated two-phase flow i.e.,

$$\begin{aligned} W^{o}_{gLi} &= W^{I}_{gLi} + W_c \\ W^{o}_{\ell Li} &= W_{ECCi} - W_c \\ T^{o}_{gLi} &= T^{o}_{\ell Li} = T_{sat} \end{aligned} \tag{42}$$

where

$$W_c = \frac{W^{I}_{gLi}\, C_{pgi}(T^{I}_{gLi} - T_{sat}) + W_{ECCi}\, C_{p\ell i}(T_{ECCi} - T_{sat})}{h_{fg}}$$

3.2.5 Downcomer annulus

The schematic of the downcomer annulus is shown in Fig. 3.3. The two-phase mixture from the intact cold legs is discharged into the upper part of the annular downcomer region. The horizontal flow path from the intact cold leg to the broken cold leg is fairly long (∿6m) and expanded in the upper downcomer annulus region in a reactor vessel. It is therefore expected that the water in the upper part of the downcomer is partly entrained to the broken cold leg by the flowing two-phase mixture even when the water level in the downcomer is below the cold leg nozzle. This bypass phenomena observed in CCTF tests[13], is considered in the code using the downcomer carry-over coefficient η_D:

$$\begin{aligned} W^o_{gA} &= W^I_{gA} + W_{gD} \\ W^o_{\ell A} &= \eta_D\, W^I_{\ell A} + W_{\ell D} \\ W_o &= (1 - \eta_D) W^I_{\ell A} \end{aligned} \tag{43}$$

where

$$W^I_{gA} = \sum_{i=1}^{N} W_{gLi}$$

$$W^I_{\ell A} = \sum_{i=1}^{N} W_{\ell Li}$$

W_{gD} and $W_{\ell D}$ is the vapor and liquid mass flow rates from the downcomer to the broken cold leg, respectively. The downcomer carry-over coefficient η_D is given as,

$$\eta_D = \begin{cases} 0 & (x < x_0) \\ \eta_{DO} & (x \geq x_0) \end{cases}, \tag{44}$$

where x is the liquid level in the downcomer, x_0 the critical liquid level above which the liquid carry over occurs. The temperature of the two-phase flow to the broken cold leg is calculated assuming the same complete homogeneous mixing as the ECC injection port described in 3.2.4.

3.2.6 Downcomer

In the present code, the downcomer component includes the downcomer and the lower plenum portion as illustrated in Fig. 3.4. The overflowing

liquid mass flow rate $W_{\ell D}$ from the downcomer to the broken cold leg nozzle is evaluated by,

$$W_{\ell D} = \begin{cases} 0 & (x < x_{max}) \\ W_o - W_c^I + W_{ECCLP} + W_{FB} & (x \geq x_{max}) \end{cases} \tag{45}$$

where x_{max} is the maximum length of the downcomer i.e. the distance from the downcomer bottom to the lower edge of the cold leg nozzle.

The steam mass flow rate W_{gD} is tentatively set equal to zero, assuming no voiding of the water in the downcomer as the zero-order approximation.

The temperature of the downcomer liquid $T_{\ell DC}$ is calculated by the mass and energy balances in the downcomer:

$$\frac{d}{dt} M_D = W_o - W^* - W_{\ell D} \quad , \tag{46}$$

$$\frac{d}{dt} \{M_D C_{p\ell}(T_{\ell D} - T_{sat})\} = W_o C_{p\ell}(T_{\ell A} - T_{sat}) - W_{\ell D} C_{p\ell}(T_{\ell D} - T_{sat}) - W^* C_{p\ell}(T^* - T_{sat}) \tag{47}$$

where $W^* = W_C^I - W_{ECCLP} - W_{FB}$,

$$T^* = \begin{cases} T_{\ell D} & (W^* \geq 0) \\ T_{\ell LP} & (W^* < 0) \end{cases}$$

Using the finite differential scheme, the downcomer liquid temperature at the next time step $T_{\ell D}^{n+1}$ is expressed as

$$T_{\ell D}^{n+1} = L \cdot T_{\ell D}^{n} + M \cdot T_{\ell A}^{n} + N \cdot T_{\ell Lp}^{n} \quad . \tag{48}$$

The coefficients L, M and N are given as follows:

$$L = \begin{cases} \dfrac{2M_D - \Delta t\, W_o}{2M_D + \Delta t\, W_o} & (W^* \geq 0) \\ \dfrac{2M_D - \Delta t (W_o - W^*)}{2M_D + \Delta t (W_o - W^*)} & (W^* < 0) \end{cases}$$

$$M = \begin{cases} \dfrac{2\Delta t \cdot W_o}{2M_D + \Delta t\, W_o} & (W^* \geqslant 0) \\ \dfrac{2\Delta t \cdot W_o}{2M_D + \Delta t(W_o - W^*)} & (W^* < 0) \end{cases} \tag{49}$$

$$N = \begin{cases} 0 & (W^* \geqslant 0) \\ \dfrac{-2\Delta t\, W^*}{2M_D + \Delta t(W_o - W^*)} & (W^* < 0) \end{cases}$$

The lower plenum is assumed to be full of liquid during the reflood phase. The energy balance in the lower plenum is then written as,

$$\begin{aligned} & M_{LP}\, C_{p\ell}\, \frac{d}{dt}\,(T_{\ell LP} - T_{sat}) \\ & = C_{p\ell}\, W^*(T_1^* - T_{sat}) + C_{p\ell}\, W_{FB}(T_{\ell U} - T_{sat}) \\ & + C_{p\ell}\, W_{ECCLP}(T_{ECCLP} - T_{sat}) - C_{p\ell}\, W_c^I(T_2^* - T_{sat}) \end{aligned} \tag{50}$$

where T_1^* and T_2^* are the liquid temperatures at the upstream i.e.,

$$T_1^* = \begin{cases} T_{\ell D} & (W^* \geq 0) \\ T_{\ell Lp} & (W^* < 0) \end{cases}$$

$$T_2^* = \begin{cases} T_{\ell Lp} & (W_c^I \geq 0) \\ T_{\ell c} & (W_c^I < 0) \end{cases} \tag{51}$$

The liquid temperature $T_{\ell Lp}$ in Eq. (50) is calculated in a similar manner as in Eq. (47) by using the finite differential scheme.

3.2.7 Broken cold leg nozzle

The two-phase mass flow rate and the fluid temperatures at the broken cold leg are calculated with the downcomer annulus component described in 3.2.5. The pressure drop across the broken cold leg nozzle ΔP_{BCN} is the differential pressure between the top of the downcomer and the exit of the broken cold leg nozzle. A farily large ΔP_{BCN} was

observed in CCTF and hence it does affect the overall system responses. The ΔP_{BCN} can be expressed by using the K-factor for the dynamic pressure drop of the two-phase mixture:

$$\Delta P_{BCN} = \{\frac{1}{2} \cdot \rho_g \cdot u_g^2 \alpha + \frac{1}{2} \rho_\ell u_\ell^2 (1 - \alpha)\} K_{BCN} \quad , \tag{52}$$

where the void fraction α, the vapor velocity u_g and the liquid velocity u_ℓ are given assuming the completely homogeneous flow with no slip:

$$\alpha = \frac{\rho_\ell W^o_{gA}}{\rho_\ell W^o_{gA} + \rho_g W^o_{\ell A}} \quad ,$$

$$u_\ell = \begin{cases} \dfrac{W^o_{\ell A}}{\rho_\ell \cdot \frac{\pi}{4} \cdot D_{BCN}^2 (1 - \alpha)} & (\alpha \neq 1) \\ 0 & (\alpha = 1) \end{cases} \quad , \tag{53}$$

$$u_g = \begin{cases} \dfrac{W^o_{gA}}{\rho_\ell \cdot \frac{\pi}{4} \cdot D_{BCN}^2 \alpha} & (\alpha \neq 0) \\ 0 & (\alpha = 0) \end{cases} \quad ,$$

and K_{BCN} is the K-factor of the broken cold leg nozzle. In the present code, the differential pressure across the broken cold leg includes all pressure losses between the top part of the downcomer and the containment (break point). This additional pressure loss is included in the K-factor K_{BCN}, which is the input of the code.

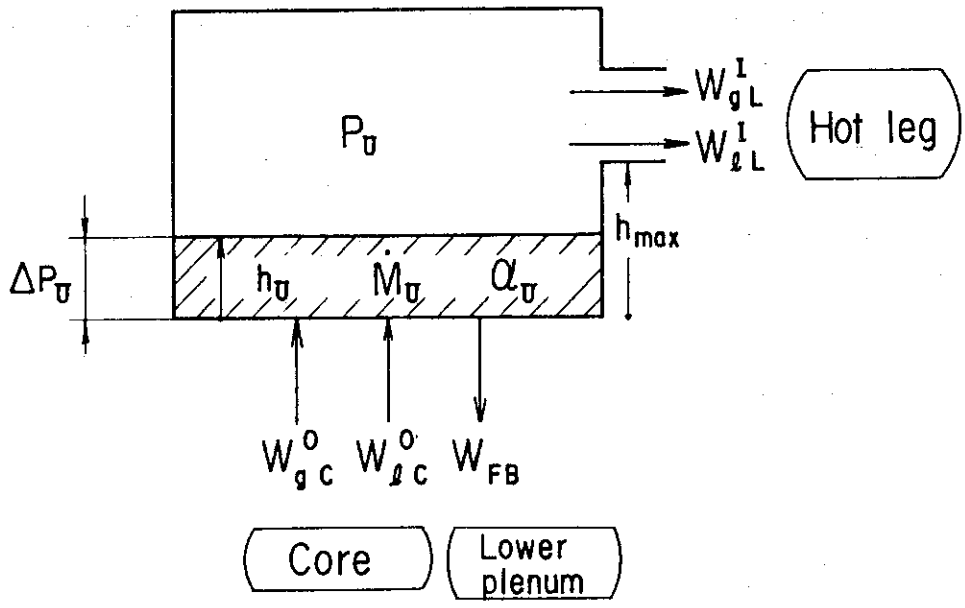

Fig. 3.1 Schematic of upper plenum

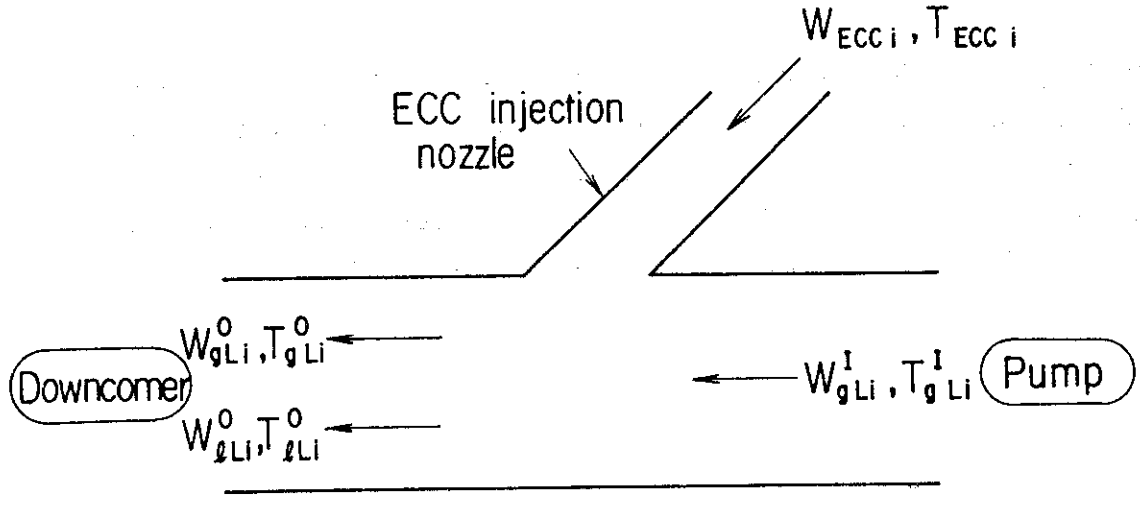

Fig. 3.2 Schematic of ECC injection port

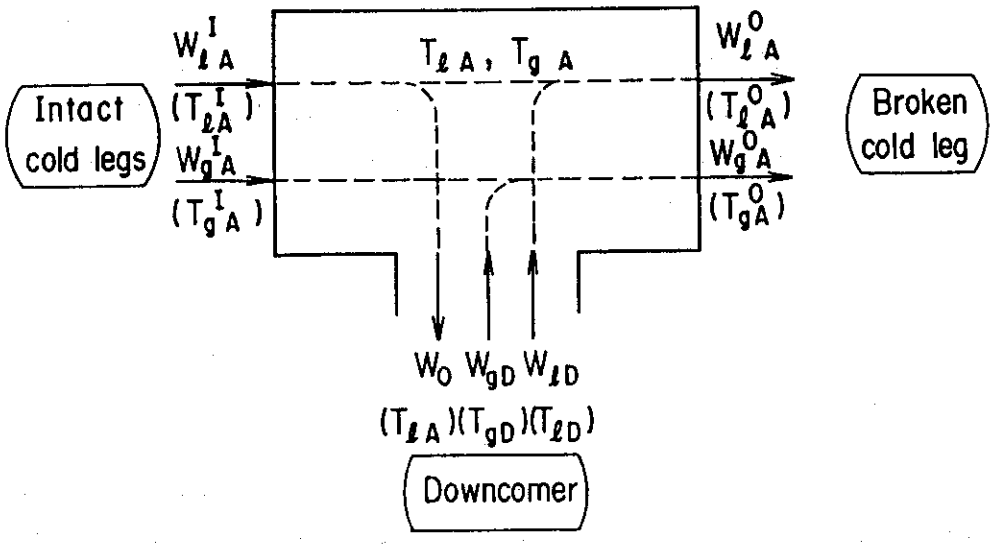

Fig. 3.3 Schematic of upper annular port of downcomer

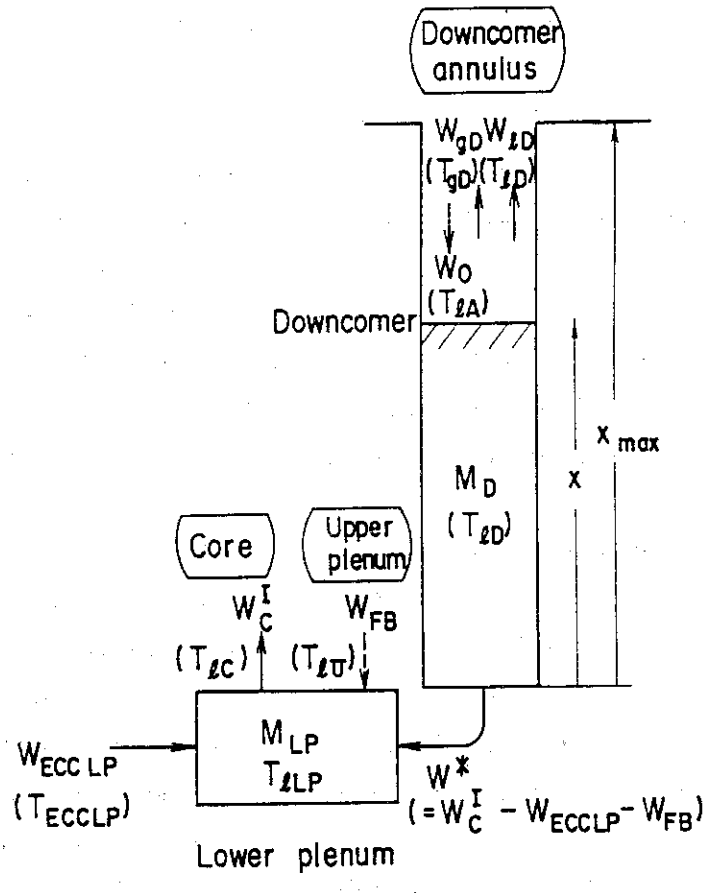

Fig. 3.4 Schematic of downcomer and lower plenum

4. Application to CCTF tests

In order to evaluate the dynamic and static characteristics of the code, REFLA-1DS was applied to the Cylindrical Core Test Facility (CCTF). The CCTF at Japan Atomic Energy Research Institute has a four-loop primary system with active steam generators and a full hight 2048 rod core. The general description of CCTF tests is given in this section.

4.1 Test facility

The CCTF is designed to simulate the flow conditions in the primay system of a PWR during the refill and reflood phases of a LOCA. The vertical dimensions of the system components are nearly the same as those of a 1000 MW-PWR with four primary loops. The flow area of the system components is based on the core flow area scaling ratio of 1:21.4.

The pressure vessel consists of an annular downcomer, upper and lower plenums, and a non-nuclear core. The core has thirty-two 8×8 rod bundles. Figure 4.1 shows the cross section of the pressure vessel and the arrangement of the instrumented heater rods in the core. The core is divided into three power zones, namely A(high power), B(medium power) and C(low power) regions, respectively, as shown in the figure. In order to simulate a local power distribution, a bundle is modeled with three types of heater rods, namely X, Y and Z rods, respectively. The heated length and the outer diameter of the heater rods are 3.66 m and 10.7 mm, respectively. The axial power profile is modeled with a 17 step chopped cosine, having the axial peaking factor of 1.49.

The facility has three intact loops and a broken loop. Each loop consists of hot leg and cold leg pipings, an active steam generator and a pump simulator. A 200% cold leg break is simulated for the broken cold leg. The broken cold leg is connected to two containment tanks. ECCS consists of an accumulator (Acc) and a low pressure coolant injection (LPCI) system. The injection points are at each cold leg and at the lower plenum. Figure 4.2 shows the schematic diagram of CCTF and the definition of the system variables. The scaled dimensions of the component are given in Table 4.1.

4.2 Test procedure

The test procedures were as follows: The lower plenum was initially filled with saturated water to 0.9 m from the bottom of the vessel. The electric power was then applied to the heater rods in the core. When a sepcified clad temperature was reached, the injection of the Acc water into the lower plenum was initiated. The power input to the rods began to decay at the reflood initiaion when the water reached the bottom of the heated length of the heater rods (2.1 m from the bottom of the vessel). The injection port was changed from the lower plenum to the three intact cold leg ECC ports at about 5 s after the reflood initiation. At about 13 s, the ECC injection mode was changed from an Accumulator (Acc) to a low pressure coolant injection (LPCI). The generated steam and the entrained water flowed via broken and intact loops to the containment tanks. The pressure of the containment tank was kept constant during the test. When all heater rod temperatures showed complete cooling of the core, the power supply to the heater rods was turned off terminating the test.

4.3 Test conditions

Table 4.2 gives the major test conditions for the CCTF base case test. In the CCTF parametric effect test series, only one test condition was varied from the base case test. The test condition of the CCTF parametric effect tests in the present code application are shown in Table 4.3.

Table 4.1 Scaled dimensions of the CCTF components

	PWR	CCTF	Ratio
< Length (m) >			
Heated length	3.66	3.66	1/1
Diameter of heated rod	10.7×10^{-3}	10.7×10^{-3}	1/1
Diameter of non-heated rod	13.8×10^{-3}	13.8×10^{-3}	1/1
Rod pitch	14.3×10^{-3}	14.3×10^{-3}	1/1
Distance from the bottom of cold leg nozzle to the bottom of the heated core	4.849	4.849	1/1
Distance from the top of the heated core to the top of the core support plate	0.357	0.357	1/1
Downcomer length	6.066	6.066	1/1
Distance from the bottom of the vessel to the bottom of the heated core	-	2.1	
< Flow area (m^2) >			
Core	5.29	0.260	1/20.3
Downcomer	2.47	0.197	1/21.4
Core baffle	1.76		
Upper plenum	11.10	0.678	1/16.4
Containment tank 1	-	4.906	
Primary loop	0.487 0.383	0.019	1/25.8 1/20.3
< Volume (m^3) >			
Lower plenum*	29.6	1.38	1/21.44
Upper plenum	43.6	2.04	1/21.44

* included the downcomer region below the bottom of core.

Table 4.2 Test conditions of the CCTF base case test

Item	Values
System pressure	0.2 MPa
Initial average linear power	1.4 kW/m
Radial power factor	1.15
Axial power factor	1.49
Local power factor	1.1
Total peaking factor	1.885
Decay curve of power	ANS × 1.2 + Actinide × 1.1
Maximum initial clad temperature	873 K
Downcomer wall temperature	471 K
Other wall temperature	392 K
Steam generator secondary side water temperature	538 K
K factor of primary loop	25
ECC injection conditions	
Acc flow rate	$7.78 \times 10^{-2} m^3/s$
Acc water temperature	308 K
Acc injection period	14 sec
LPCI flow rate	$8.33 \times 10^{-3} m^3/s$
LPCI water temperature	308 K

Table 4.3 Parametric effect tests in CCTF

Test parameter		Test number
System pressure (MPa)	0.15	C1-10
	0.20	C1-5
	0.30	C1-12
ECC injection rate ($\times 10^{-3} m^3/s$)		
Acc	77.2(×14 s)	C1-5
LPCI	8.3	C1-5
High LPCI	17.2	C1-6
Low LPCI	4.7	C1-9
Initial peak clad temperature (K)	873	C1-5
	973	C1-7
	1073	C1-14

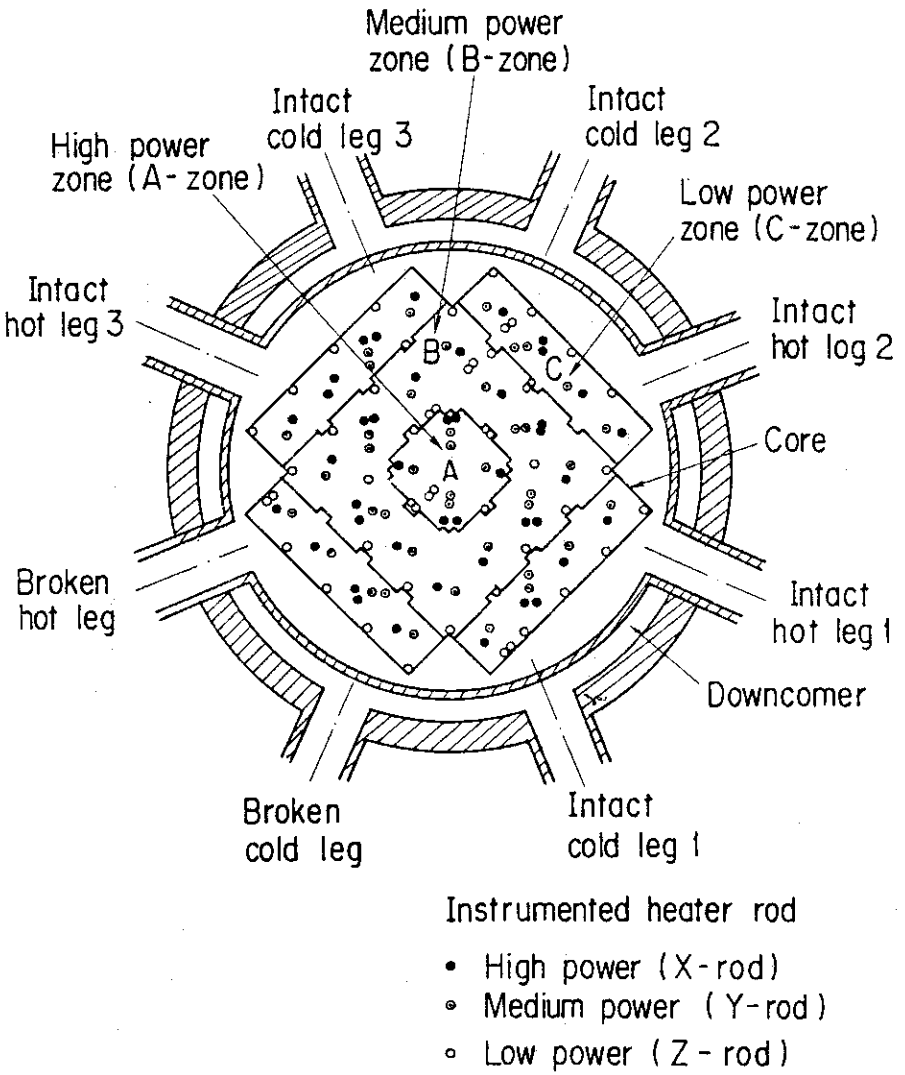

Fig. 4.1 Cross section of CCTF pressure vessel

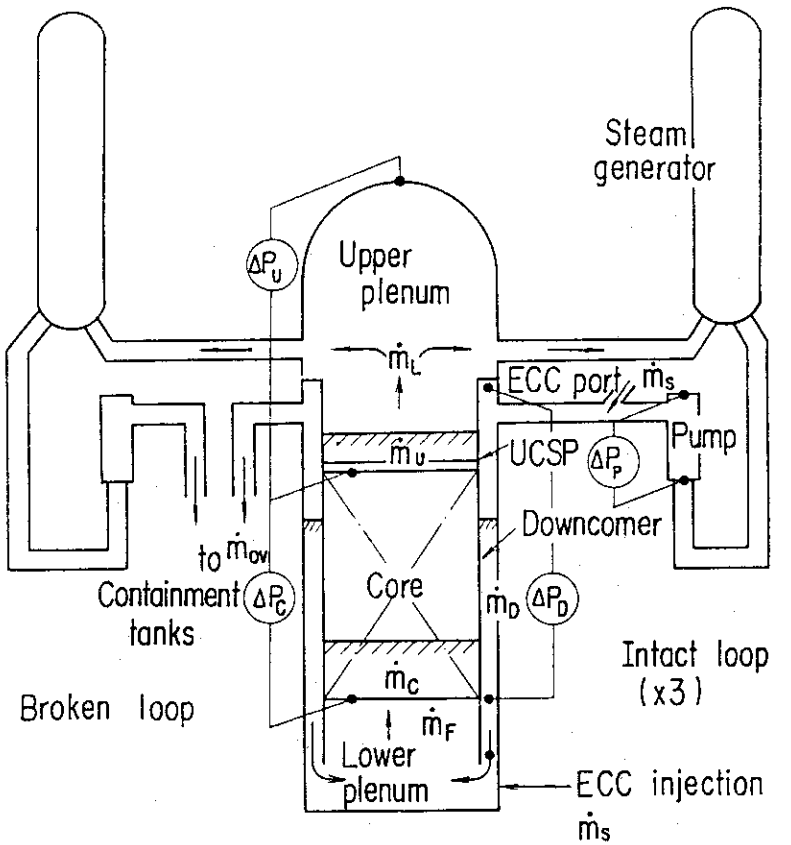

Fig. 4.2 Schematic of CCTF system and locations of differential pressure measurement

5. Calculated results and discussion

5.1 Base case calculation

The base case calculation was performed in order to evaluate the thermo-hydraulic models used in the code and to further investigate the effect of the calculative parameters on the overall system responses. The analytical calculation performed was for CCTF Test C1-5, which is the base case test in CCTF Core I test series. The code inputs and the selected parameters for the CCTF base case calculation are summarzied in Table 5.1.

5.1.1 Overall system responses

The calculated flooding rate and collapsed water levels in the core, downcomer and upper plenum are compares with the measured data in Fig. 5.1. The flooding rate in the experiment was estimated with the mass balance in the system using the smoothed differential pressure measurement. As shown in Fig. 5.1, the calculated results agree well with the measured data on an average. However, the calculated water level in the core before about 25 s is higher than the experiment. This is primarily due to the calculated lower steam generation rate and carry-over water before 25 s in the core region than the experiment. This then causes the smaller steam binding in the primary loop, resulting in the higher flooding rate into the core before 25 s than the experiment as shown in Fig. 5.1. The water accumulation in the upper plenum initiates after about 25 s, showing the delayed water carry-over at the exit of the core.

Figure 5.2 shows the calculated and measured pressure drops across the primary loop. The calculation generally agrees well with the measured on an average. The calculated broken and intact loop pressure drops are lower than the measured before about 25 s. This calculated smaller steam binding is again due to the smaller steam generation and carry-over in an early reflood transient.

Figure 5.3 shows the measured and calculated fluid temperatures at the core inlet. Although the calculated temperature is about 10 K lower than the measured, the overall tendency is well predicted. Also shown in the figure is the measured core inlet temperature in the CCTF test with the cold downcomer. The temperature of the cold downcomer

test was about the saturation temperature. The calculated core inlet temperature agrees better with the case of the cold downcomer test after about 100 s through the transient. This is therefore due to the lack of the heat generation model from the downcomer wall in the present code. It is considered, however, that the effect of the inlet subcooling in this range is negligible on the overall core and system behaviors. The slightly higher core inlet temperature before 100 s is not fully understood. This is probably due to the unhomogeneous mixing of the water in a complicated configuration of the structure in the lower plenum, which is not modeled in the code.

Figure 5.4 shows the measured and calculated temperature histories of the heated rod in the core. The overall temperature histories are well predicted by the code. The calculated turnaround temperature is slightly lower than the measured in the upper part of the core. It is considered that this is due to the sudden core cooling at about 10 s shown by an arrow in Fig. 5.4 due to the higher core flooding rate shown in Fig. 5.1. The calculated quench time tends to be slightly later than the measured in the upper part of the core. This can be attributed to the lack of the appropriate top-down quenching model in the present code.

The void fraction in the core is shown in Fig. 5.5. The measured void fraction was obtained with the sectional differential pressure in the core neglecting the frictional pressure loss. The calculated void fraction shows good agreement with the measured except for the top part of the core. Before about 20 s of the transient, the calculated void fraction is much lower than the measured. This is due to the calculated higher initial core flooding rate shown in Fig. 5.1. The cause of the calcualted smaller water accumulation in the top of the core is due to the core inlet flow oscillation, which tends to sweep the accumulated water in the region of the high void fraction.

5.1.2 Upper plenum de-entrainment

The effect of the de-entrainment coefficient η_U in Eq. (27) on the water accumulation in the upper plenum was investigated. As shown in Fig. 5.6, the water accumulation in the upper plenum is lower with the larger η_U especially in the early reflood transient before about 150 s. However the effect of η_U is not sensitive in the range between 0.4 to 0.8. Also the effect of η_U on the core collapsed water level is

almost negligible as shown in Fig. 5.6. The recommended value of 0.6[15] is adopted for η_D in the present base case calculation.

5.1.3 Loop K-factor

The loop K-factor K_{Li} in Eq. (35) was parametrically varid in order to analytically estimate K_{Li} in CCTF. The loop pressure drop is slightly higher with the higher loop K-factor as shown in Fig. 5.7. However the effect on the core cooling is not dominant as shown in the figure. The slightly worse core cooling for K_L = 20 is due to the larger oscillation, which is discussed in section 5.1.6. The estimated loop K-factor is in the range of 20 to 30 according to the mass balance calculation. Tentatively a value of 25 is adopted in the base case calculation, however, the direct measurement of the loop K-factor in situ is required for the detailed analysis of the CCTF system behavior.

5.1.4 Downcomer carryover

The downcomer carry-over coefficient η_{Do} in Eq. (44) was parametrically varied in the calculation. The carry over in the downcomer, which may be the characteristic feature of the annular type downcomer as in a PWR vessel, is larger with the larger η_{Do} resulting in the lower water level in the downcomer as shown in Fig. 5.8. The calculation with η_{Do} = 0.5 gives a better agreement with the data as shown in Fig. 5.8, and hence it is used in the calculation.

5.1.5 Broken cold leg

The K-factor of the broken cold leg nozzle K_{BCN} in Eq. (52) includes all the loss coefficients of the broken cold leg between the top part of the downcomer and the containment. The parametric calculation was performed to analytically estimate K_{BCN} in CCTF. As shown in Fig. 5.9, the value of 4.5 gives better agreement with the measured pressure drop across the broken cold leg.

5.1.6 Core inlet flow oscillation

The calculated core flooding rate generally oscillates in the present U-tube type schematic shown in Fig. 2.1. The source of the oscillation is the fluctuation of the outlet variables such as W^o_{gc} and $W^o_{\ell c}$ in Eq. (2). This then causes the U-tube flow oscillation of the fluid between the downcomer and the core. The period of the

oscillation is determined with the length of the liquid column. The oscillation can be enhanced due to the resonance of the U-tube flow and the core outlet flow oscillations.

Since the core model has been developed with the constant feed experiment, the oscillation with a small amplitude is favorable for the core thermo-hydraulic calculation. It is considered that the flow oscillation in the core is effectively damped in an actual reactor vessel due to the three-dimensional configuration, however, the typical value of the amplitude is uncertain.

The parametric calculation was performed in order to investigate the effect of the flow oscillation on the core heat transfer. In the calculation, the primary system was decoupled and the oscillatory core inlet flow was fed as a core boundary condition. The amplitudes of the oscillation tested were 0, 2 and 4 cm/s and the periods of the oscillation were 3 and 5 sec with the average flooding rate of 3 cm/s.

As shown in Fig. 5.10, the calculated maximum temperature is higher with the larger amplitude, but it is only slightly higher with the shorter period of oscillation. The quench time tends to be later with the larger amplitude in the upper part of the core. According to the experiments at ERSEC[17], the core heat transfer is not much affected by the flow oscillation. By comparing the calculation with the temperature transient obtained in CCTF test, it is indicated that the large core inlet flow oscillation should be avoided to reasonably predict the temperature response with the present core model.

5.2 Parameter effect

The parametric calculation was performed in order to evaluate the thermo-hydraulic models concerning the parametric effect of the system variables on the reflood behaviors. The analytical calculation performed was for CCTF parametric effect tests lited in Table 4.3.

5.2.1 System pressure

Figure 5.11 shows the effect of the system pressure on the differential pressure across the loop. As shown in the figure, the loop pressure drop is lower with the higher system pressure primary due to the larger vapor density. Although the calculated loop pressure drop is lower before about 50 s than the measured, the overall tendency is well

predicted by the code on an average.

The quench envelope in the core is compared with the data in Fig. 5.12. The core cooling is enhanced with the larger system pressure both in the experiment and the calculation. The quench time at the midplane (1.83 m) is fairly well predicted, however, the calculated quench time tends to be slightly later in the upper part of the core. It is considered that this is due to the effect of the top-down quenching observed in the test, which is not effectively modeled in the present core model. However, this is not a fatal problem for the safety analysis, since the bottom quenching region is dominant where the peak clad temperature is realized.

5.2.2 ECC flow rate

Figure 5.13 shows the effect of the ECC flow rate on the collapsed water level in the downcomer. The ECC flow rate affects the water accumulation in the downcomer. As shown in Fig. 5.13, the water level in the downcomer is higher with the higher LPCI flow rate.
The observed water accumulation in CCTF downcomer is well predicted as shown in Fig. 5.13.

5.2.3 Initial clad temperature

Figure 5.14 shows the effect of the initial clad temperature on the temperature history at the midplane. The higher initial clad temperature resulted in the higher turnaround temperature and the later quench time as shown in Fig. 5.14. Although the calculated quench time agrees well with the measured, the calculated turnaround temperature is underpredicted. This is partly because of the higher initial higher flooding rate as discussed in section 5.1, and partly because of the overpredicted heat transfer coefficient near the turnaround. Therefore the heat generation in an early transient and also the heat transfer model should be reviewed in detail for the better prediction.

Table 5.1 Code inputs and selected parameters for CCTF calculation

Variable	Description	Used value
(1) Flow area (m^2)		
A_C	Core	0.26
A_D	Downcomer	0.197
A_I	Core-downcomer connection	0.7905
A_{Ii}, A_B	Primary loop	0.01897
A_U	Upper plenum	0.64
(2) Volume (m^3)		
V_{up}	Upper plenum	9.01[1)]
(3) Length (m)		
x_{Do}	Downcomer	4.849
x_o	Effective downcomer length	3.3
L_I	Core-downcomer connection	2.1
(4) K-factor (-)		
K_L	Loop	25
K_{BCN}	Broken cold leg	4.5
K_C	Core	15
K_D	Downcomer	5
K_I	Core-downcomer connection	10
(5) Constants		
η_U	Upper plenum de-entrainment	0.6
η_{Do}	Downcomer carry over	0.5

Note 1) Includes all volume in the primary loops

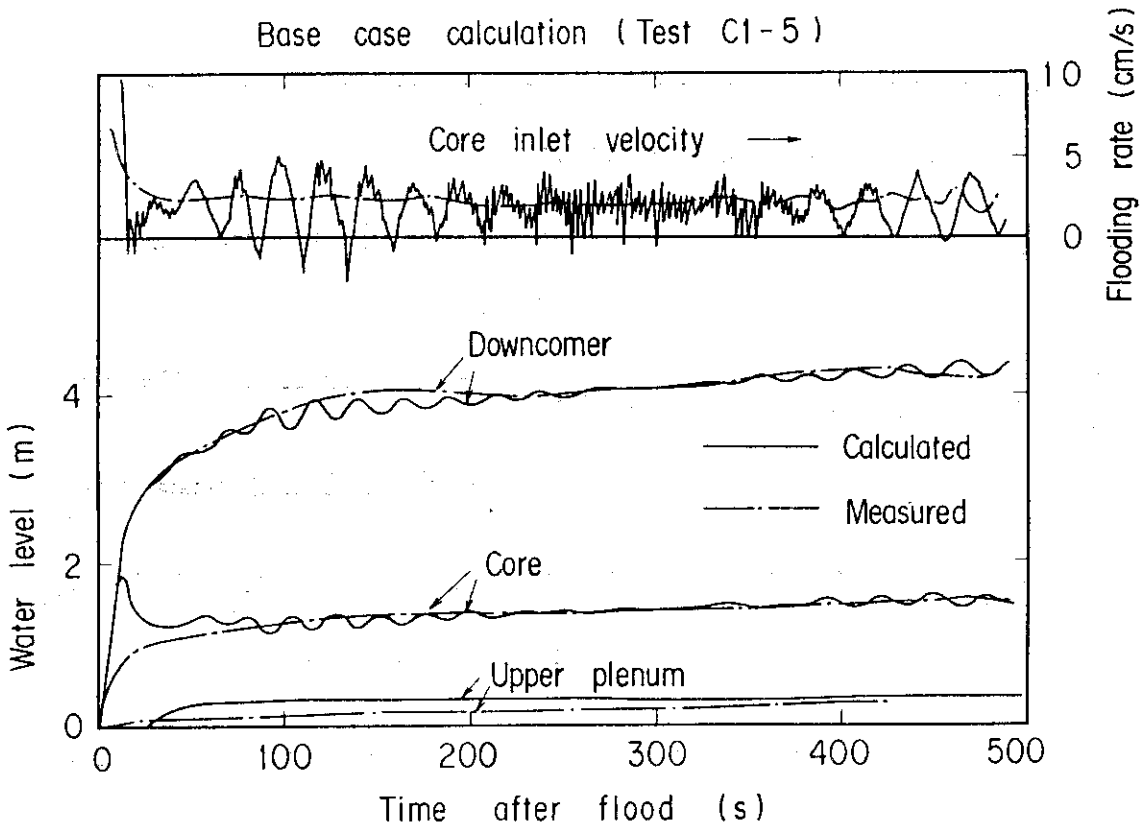

Fig. 5.1 Core flooding rate and water levels in base case calculation

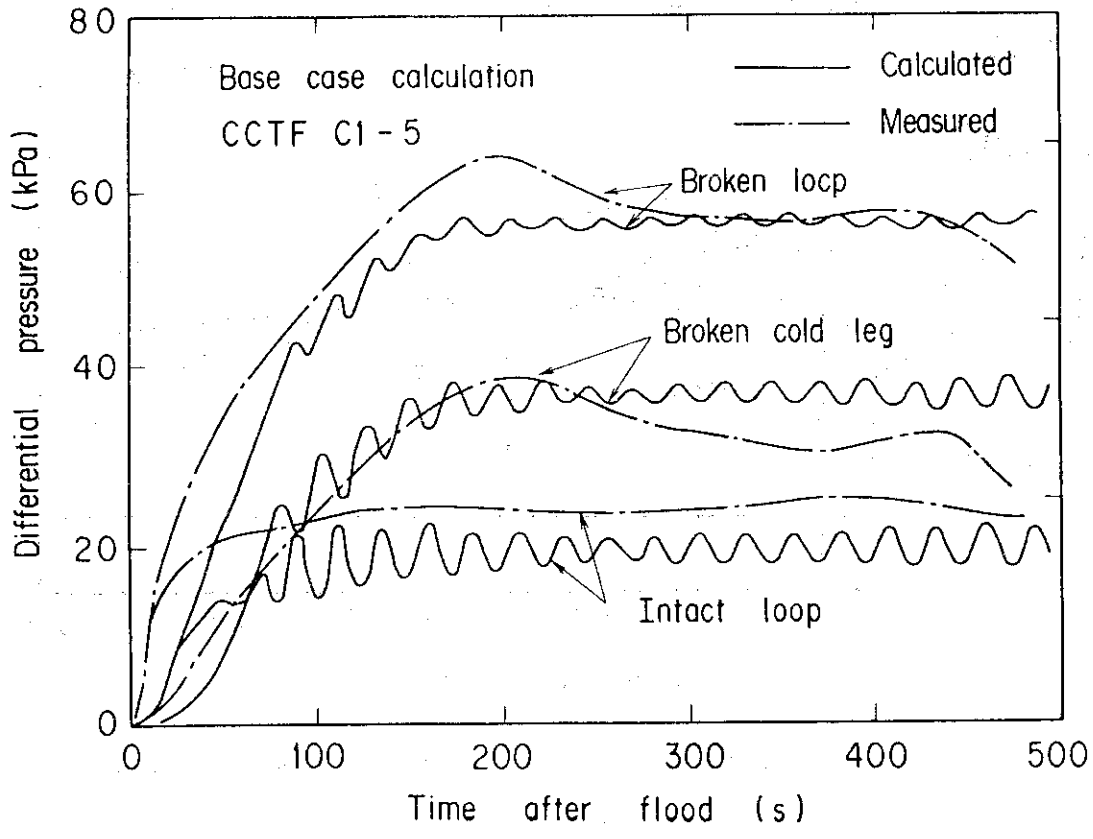

Fig. 5.2 Loop pressure drops in base case calculation

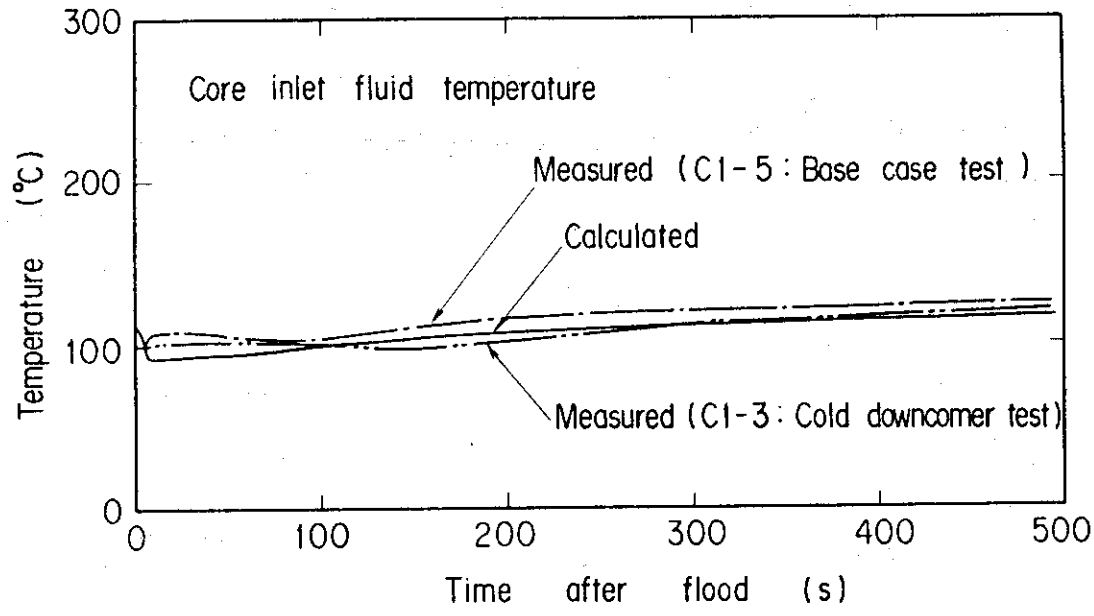

Fig. 5.3 Fluid temperature at core inlet in base case calculation

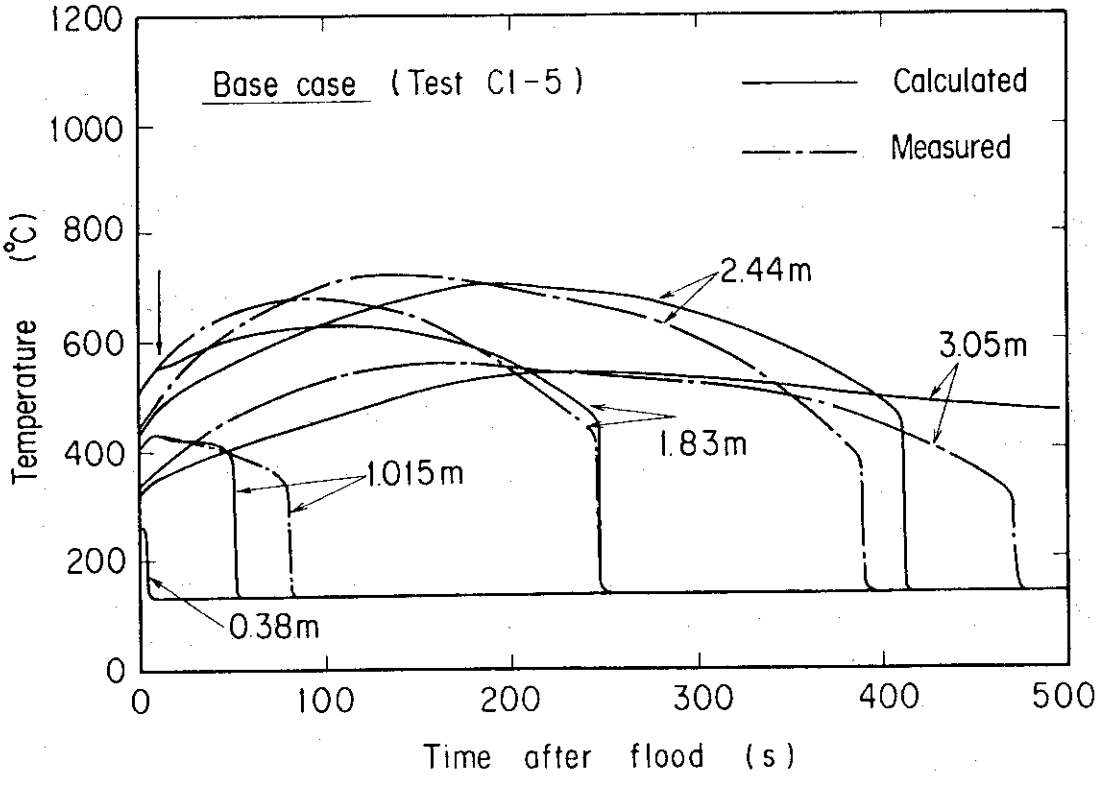

Fig. 5.4 Clad temperature in core in base case calculation

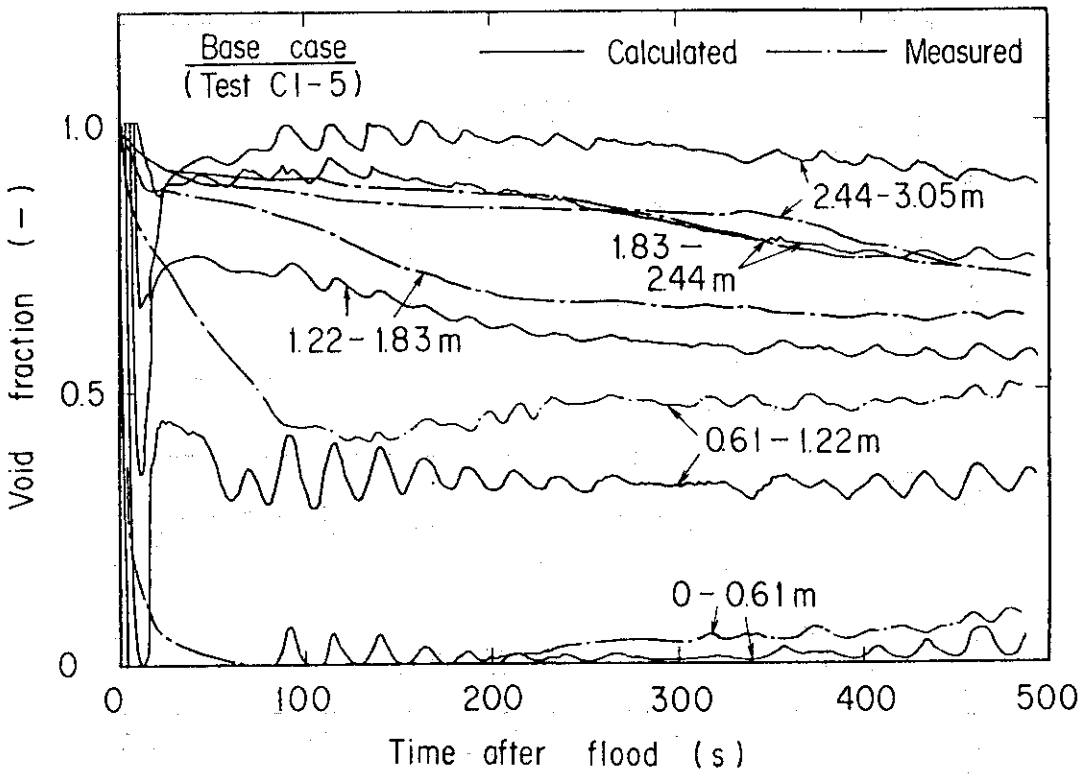

Fig. 5.5 Void fraction in core in base case calculation

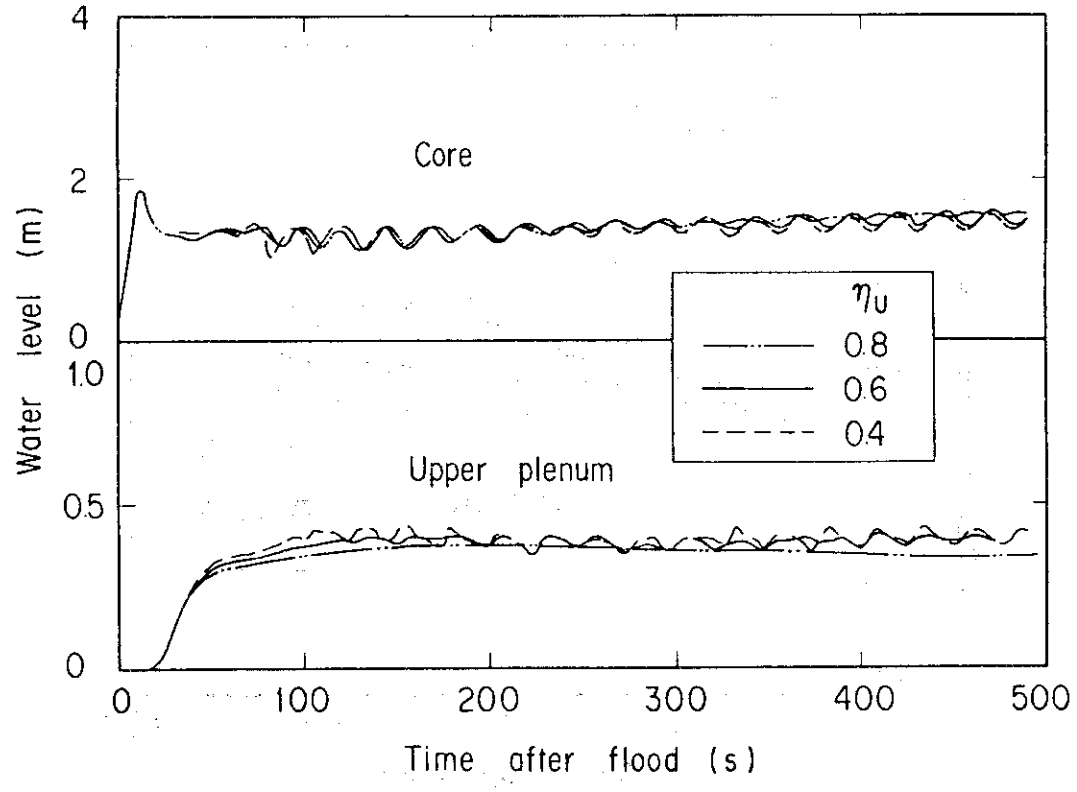

Fig. 5.6 Effect of de-entrainment coefficient on water accumulation in upper plenum

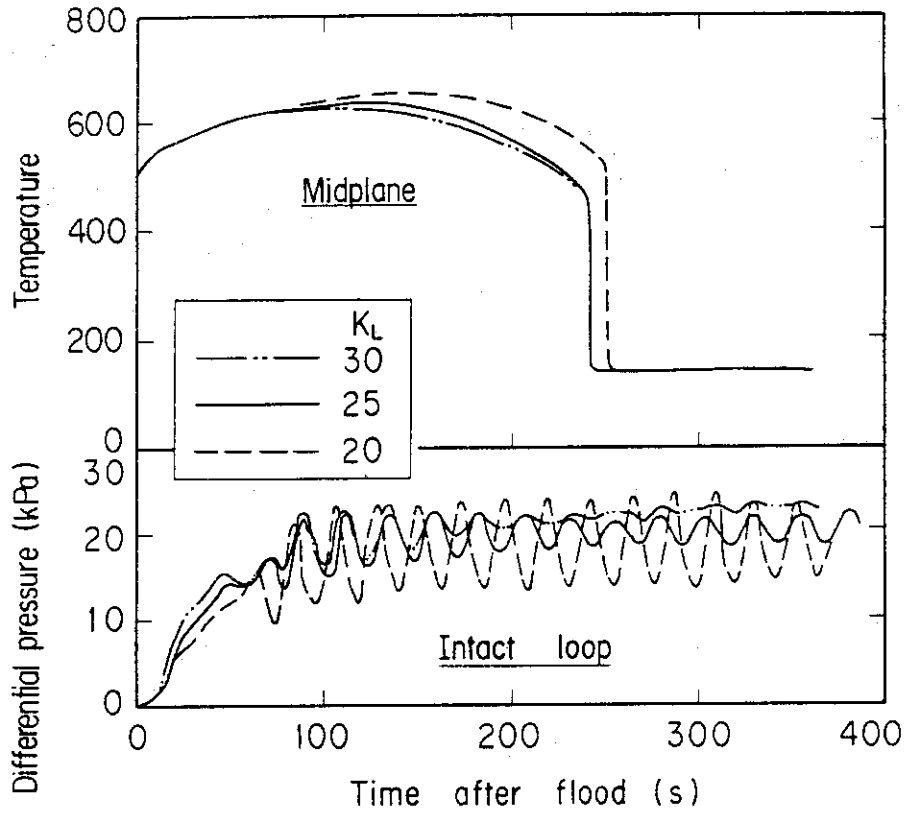

Fig. 5.7 Effect of loop K-factor on core cooling and loop pressure drop

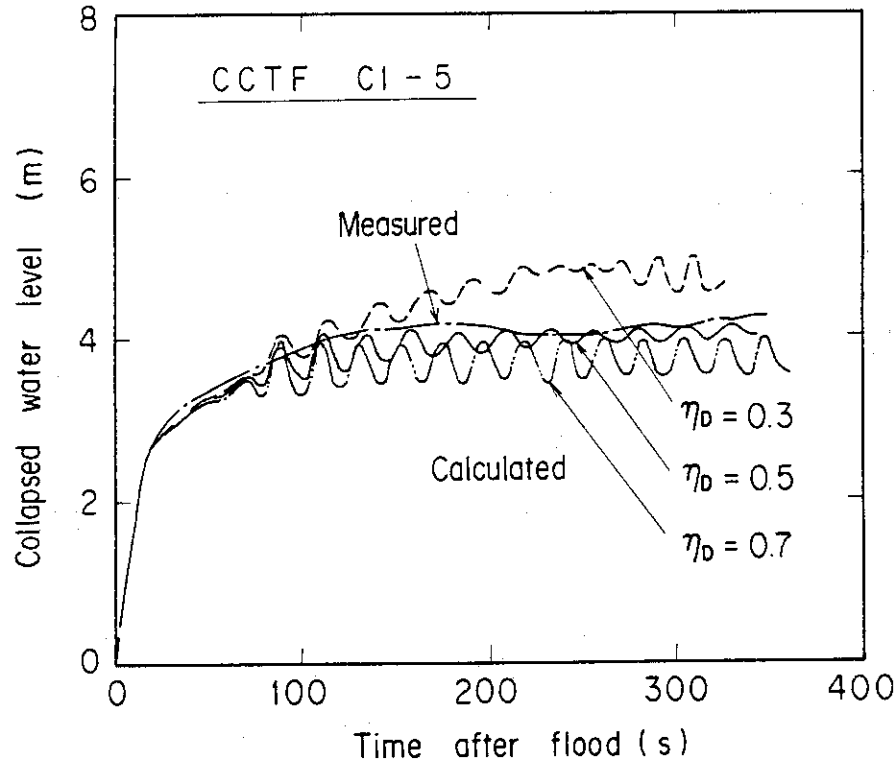

Fig. 5.8 Effect of downcomer carry over coefficient on water level in downcomer

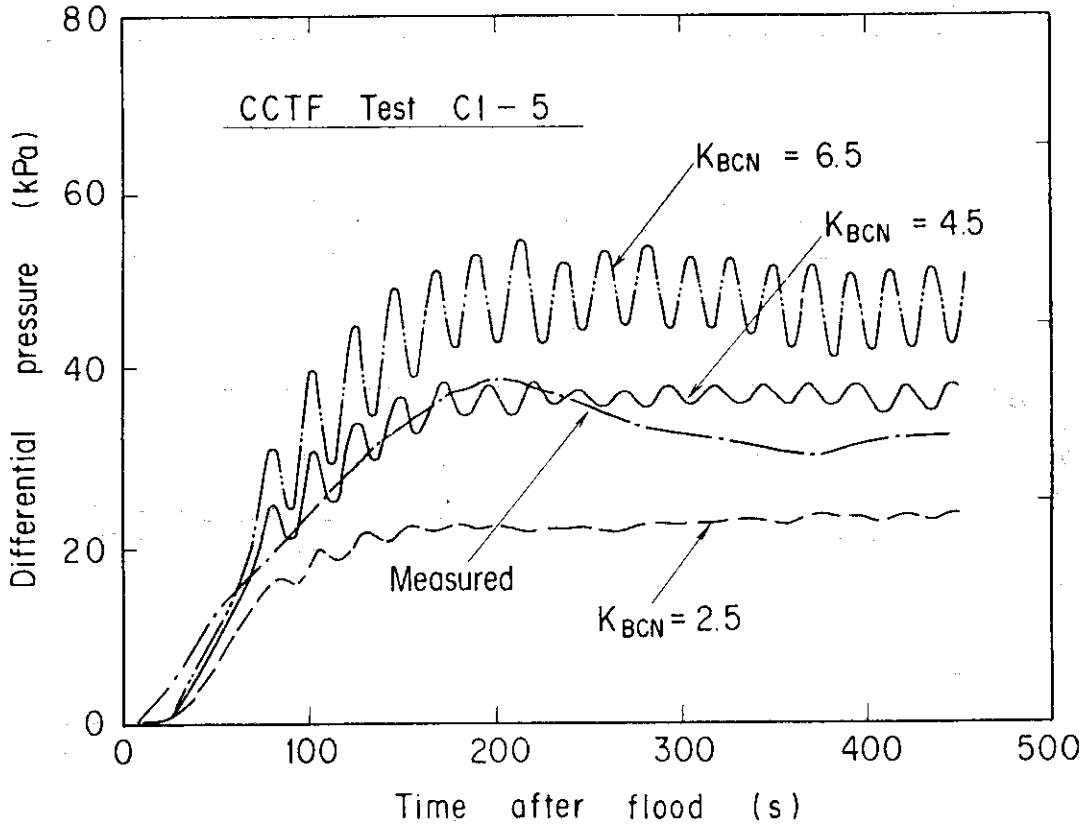

Fig. 5.9 Effect of K-factor of broken cold leg on broken cold leg pressure drop

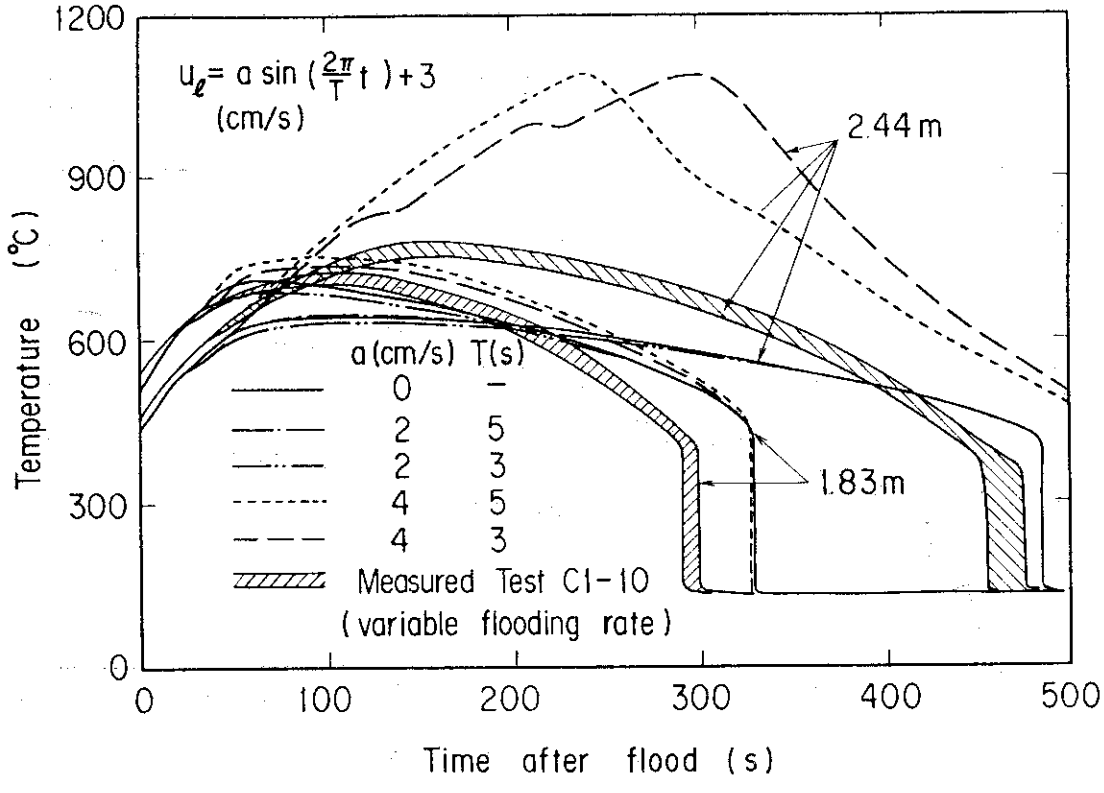

Fig. 5.10 Effect of oscillation on core cooling

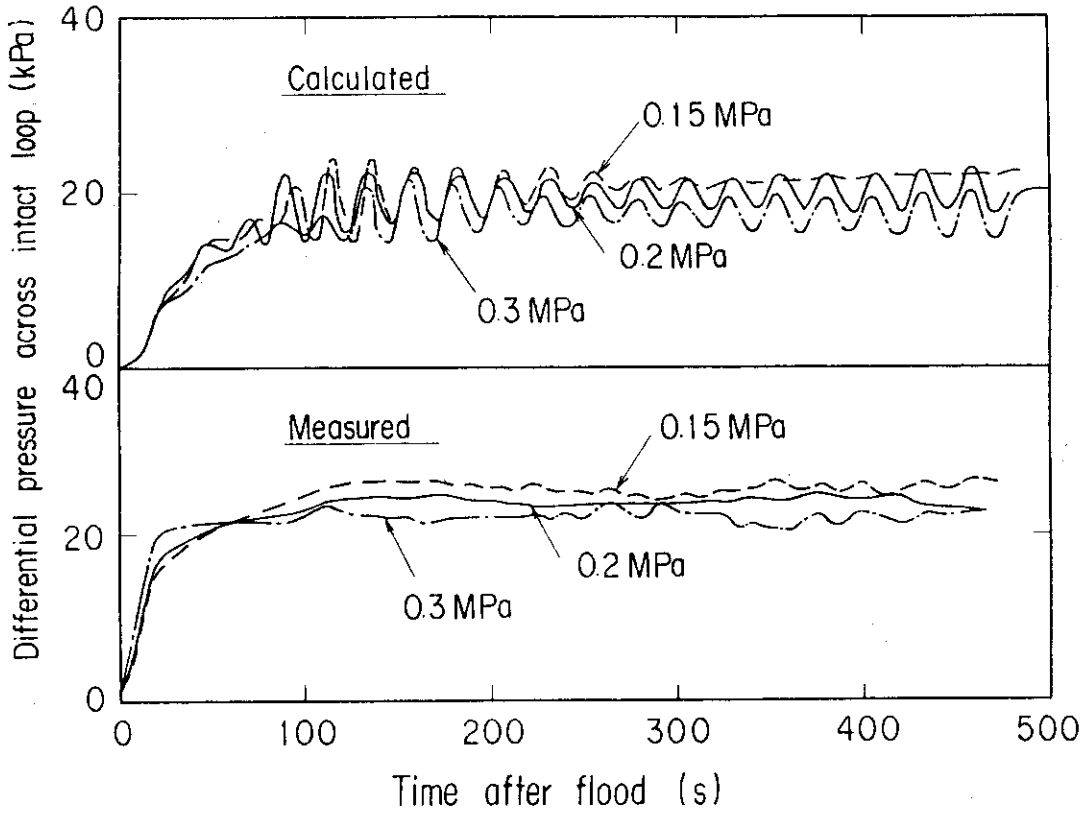

Fig. 5.11 Effect of system pressure on intact loop pressure drop

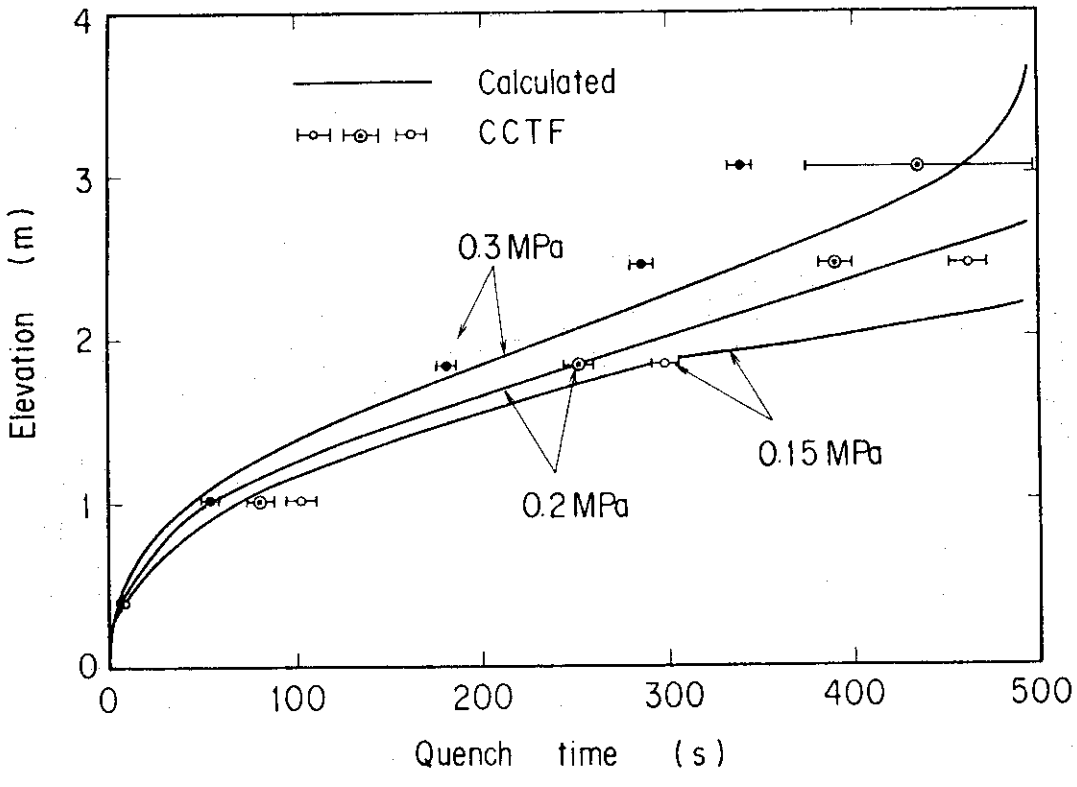

Fig. 5.12 Effect of system pressure on quench envelope

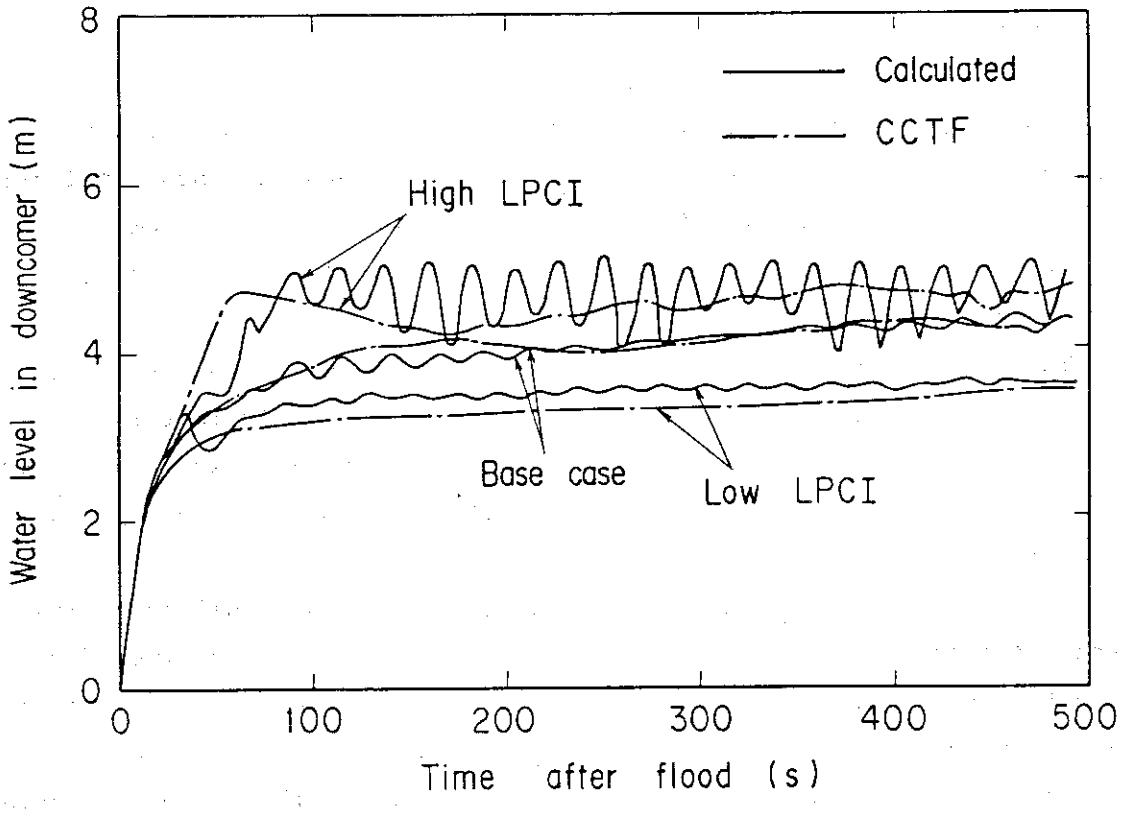

Fig. 5.13 Effect of ECC flow rate on water level in downcomer

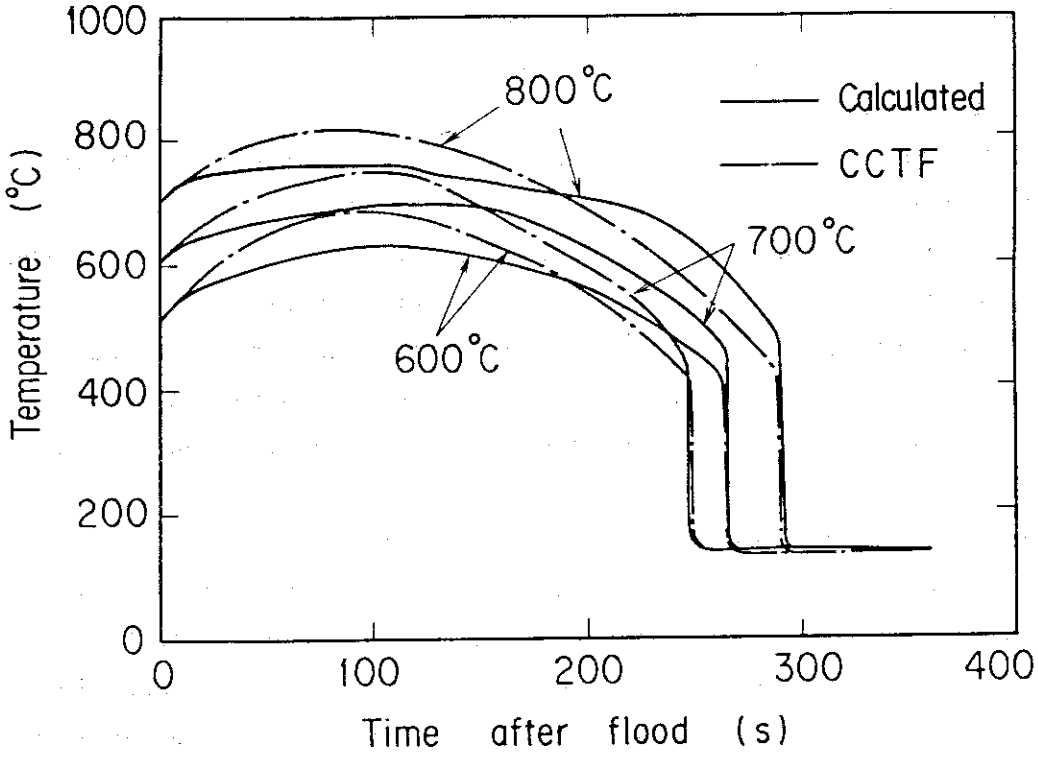

Fig. 5.14 Effect of initial clad temperature on clad temperature at midplane

6. Summary

The REFLA-1DS was developed for the system analysis of the reflood phase of PWR-LOCA. The code consists of a one-dimensional non-equilibrium two-phase core model and a multi-loop system models. The system components modeled are the upper plenum, the downcomer, the ECC injection port and the broken cold leg nozzle.

The coupling between the one-dimensional core model and the multi-loop system model is accomplished by the use of the equivalent flow resistance in a single loop with saturated steam system. The calculated core outlet variables are numerically smoothed to aoivd the unphysical oscillation.

The code was applied to the Cylindrical Core Test Facility (CCTF) tests. A fairly good agreement with the experiments was obtained for the water accumulations in the downcomer, the core and the upper plenum, and for the thermo-hydraulic behavior in the core. Also obtained was a qualitatively good agreement for the parameters of the system pressure, ECC flow rate and the initial clad temperature.

Needs for further code improvements were pointed out based on the pressure analytical investigation by comparing with CCTF data. The shortcomings of the code are summarized below:

(A) In the core model

(1) Delayed generation of the steam and the water carry-over into the upper plenum.

(2) Underpredicted quench front velocity for the upper part of the core or the lack of the top-down quenching model.

(3) Overpredicted heat transfer coefficient near the turnaround resulting in the underpredicted turnaround temperature.

(4) Strong dependence of the core inlet flow oscillation on the core cooling

(B) In the system model and the coupling method

(1) No heat release from the downcomer wall to the fluid resulting in the underpredicted water temperature at the core inlet.

(2) Strong dependence of the change of the core outlet mass flow rate on the dynamical system responses, which tends to cause an unstable system calculation.

For the application to an actual PWR, it is further necessary to model the nuclear fuel such as the gap conductance between the cladding

and the fuel element, which can affect the quench front movement.[18] Also required is the mechanical modeling of the system model independent of the specific test facility, especially for the models of the de-entrainment phenomena in the downcomer.

Acknowledgement

The authors would like to express their thanks to Dr. M. Nozawa, Deputy Director General of Tokai establishment, Dr. S. Katsuragi, Director of Nuclear Safety Research Center, and Dr. K. Hirano, Deputy Director of Department of Nuclear Safety Research for their guidance and encouragement.

They would like to express their thanks to the members of the analysis group, especially to Messrs. T. Iguchi, K. Okabe, Dr. H. Akimoto and Mr. T. Okubo for their devoted help on the model development and the CCTF data analysis.

and the fuel element, which can affect the quench front movement.[18] Also required is the mechanical modeling of the system model independent of the specific test facility, especially for the models of the de-entrainment phenomena in the downcomer.

Acknowledgement

The authors would like to express their thanks to Dr. M. Nozawa, Deputy Director General of Tokai establishment, Dr. S. Katsuragi, Director of Nuclear Safety Research Center, and Dr. K. Hirano, Deputy Director of Department of Nuclear Safety Research for their guidance and encouragement.

They would like to express their thanks to the members of the analysis group, especially to Messrs. T. Iguchi, K. Okabe, Dr. H. Akimoto and Mr. T. Okubo for their devoted help on the model development and the CCTF data analysis.

[Nomenclature]

A : Flow area (m^2)
C_p : Sepecific heat (J/kg)
D_d : Droplet diameter (m)
D_k : Diameter of holes in upper plenum tie plate (m)
d_k : Thickness of the hole in upper plenum tie plate (m)
E : Emissivity (-)
g : Acceleration of gravity (m/s^2)
h_{fg} : Latent heat of evaporation (J/kg)
h' : Water head (m)
K : Flow resistance coefficient (K-factor) (-)
L : Length (m)
M : Accumulated mass (kg)
$\dot{M}$: Mass accumulation rate (kg/s)
N : Number of intact loops
P : Pressure (Pa)
P_o : System pressure at containment (Pa)
T : Temperature (K)
t : Time (s)
U : Velocity (m/s)
V_u : Volume of upper plenum (m^3)
W : Mass flow rate (kg/s)
W_{ec} : Critical Weber number (-)
X : Set of variables (x, y, U_I, P_D, P_I)
x : Liquid level in downcomer (m)
y : Liquid level in core (m)
α : Void fraction (-)
ΔP : Differential pressure (Pa)
ΔT_{sub} : Liquid subcooling (K)
Δt : Time step (s)
ΔU : Slip Velocity (m/s)
η_D : Downcomer carry-over coefficient (-)
η_U : Upper plenum de-entrainment coefficient (-)
ρ : Density (kg/m^3)
σ : Surface tension (kg/m)

Subscripts

A	:	Downcomer annulas
B	:	Broken loop
BCN	:	Broken cold leg nozzle
C	:	Core
c	:	Critical
D	:	Downcomer
ECC	:	ECC port
ECCLP	:	ECC injected in lower plenum
FB	:	Fallback
g	:	Gas phase
h	:	Hole
I	:	Inlet (Upper suffix); Intact loop (Lower suffix)
i	:	i-th intact loop
L	:	Primary loop
LP	:	Lower plenum
ℓ	:	Liquid phase
max	:	Maximum
n	:	time at $t = t$
n+1	:	time at $t = t + \Delta t$
O	:	Outlet (Upper suffix)
Q	:	Quench
S	:	System
sat	:	Saturation
U	:	Upper plenum

References

(1) Murao, Y.: Analytical study of thermo-hydrodynamic behavior of reflood-phase during LOCA, J. Nucl. Sci. Technol. 16[11], 802 ∿ 817 (1979).

(2) Murao, Y.: Development of multi-loop system model by using CCTF data, JAERI-M to be published.

(3) Cermak, J.O., et al.: PWR full length emergency cooling heat transfer (FLECHT) group I test report, WCAP-7435, (1970).

(4) Murao, Y., et al.: CCTF Core I test results, JAERI-M 82-073 (1982).

(5) Adachi, H., et al.: SCTF Core I test results, JAERI-M 82-075 (1982).

(6) Murao, Y., et al.: One-dimensional system analysis code for reflood phase during LOCA, JAERI-M 9780 (1981).

(7) Sudoh, T., et al.: Data report or reflood experiment VII (Series 6, Intermittent flow rate core forced injection test and system effect tests), JAERI-M 8162 (1979) (In Japanese).

(8) Murao, Y., et al.: REFLA-1D/mode 3: A computer program for reflood thermo-hydrodynamic analysis during PWR-LOCA (User's mannual), JAERI-M to be published.

(9) Murao, Y.: Study of the thermo-hydrodynamic phenomena in the nuclear core during reflood phase, JAERI-M 83-032 (1983) (In Japanese)

(10) Murao, Y.: Quench model for lower temperature than thermohydro-dynamic maximum liquid superheat, JAERI-M 10000 (1982). (In Japanese)

(11) Murao, Y.: Correlation of quench phenomena for bottom flooding during loss-of-coolant accidents, J. Nucl. Sci. Technol., 15 [12], pp. 875 ∿ 885, (1978).

(12) Waring, J.P., et al.: PWR FLECHT-SET phase B1 evaluation report, WCAP-8583, (1975).

(13) Murao, Y., et al.: Experimental study of system behavior during reflood phase of PWR-LOCA using CCTF, J. Nucl. Sci. Technol. 19 [9] pp. 705 ∿ 719 (1982).

(14) Bankoff, S.G., et al.: Steam-water mixing studies, presented at seventh Water Reactor Safety Research Information Meeting, Washington D.C. (1979).

(15) Iguchi, T., et al.: Water accumulation phenomena in upper plenum during relood phase of a LOCA by using CCTF data, T. Nucl. Sci. Technol. 20[6], 453 ~ 466 (1983).

(16) Wilson, J.F., et al.: The velocity of rising steam in a bubbling two-phase mixture, Trans. ANS, Vol. 5, 151, (1962).

(17) Clement, P., et al.: Reflooding of a PWR bundle: Effect of inlet flow oscillations and spacer grid, presented at European Two Phase Flow Group Meeting, Paris (1982).

(18) Sudoh, T.: Investigation of typicality of non-nuclear rod and fuel-clad gap effect during reflood phase, and development of a FEM thermal transient analysis code HETFEM, JAERI-M 9533 (1981).